International

WOCE

Newsletter

Number 27 July 1997

IN THIS ISSUE

Published by WOCE International Project Office at Southampton Oceanography Centre, UK

Guest Editorial

W. Lawrence Gates (Chairman, JSC/WCRP). Larry.Gates@quickmail.llnl.gov

Although I have long been aware of the scientific challenges in oceanography and of the oceans' important interactions with the atmosphere on climate timescales (and have, in fact, done some modelling research on these subjects in the late 1960s and early 1970s), I had not begun to appreciate the scope and usefulness of WOCE until I chaired the JSC Steering Group on Global Climate Modelling in the early 1990s and chaired the JSC itself since 1994. I am therefore particularly pleased to have been asked to write this editorial, and to express my views on the role and importance of WOCE in the WCRP.

WOCE is, without doubt, the most ambitious oceanographic research project yet undertaken, and promises to provide a unique observational data set of the state of the global ocean during the early and mid-1990s, along with significant advances in our ability to model the ocean. While the set of hydrographic and chemical measurements made on a global network of zonal and meridional sections are perhaps the data most often associated with WOCE, the direct current measurements (including data from current meter moorings, subsurface floats, surface drifting buoys, and acoustic Doppler current profiles) collected under WOCE auspices are a valuable supplement to the one-time WOCE hydrographic survey and selected repeat sections. Other WOCE data that are of direct use in studying ocean-atmosphere interaction are the upper ocean and sea surface observations (including upper ocean thermal data, sea surface salinity, in situ sea level data, and surface meteorological data and surface fluxes). A more synoptic view of the ocean is provided by the global measurements made by satellites such as the TOPEX/POSEIDON, NSCAT and the ERS series, and although not now collated and distributed by WOCE, these data promise to revolutionize our knowledge of ocean behaviour. The WOCE data collection and associated data management system will be a valuable resource for continuing research on ocean data assimilation and operational prediction of the coupled ocean-atmosphere system.

WOCE has also played an important role in the advances in ocean modelling that have taken place in recent years. Although most coupled global ocean-atmosphere models continue to use relatively coarse resolution (due to computer limitations), WOCE has promoted the development of very high resolution models on both basin and global scales and the development of new formulations such as the use of isopycnal, terrain-following and finite element coordinates. Such models have found important application in studies of the structure and circulation on regional scales that are important in the ocean's vertical and horizontal transport of heat and water. In this research WOCE has an intersection with the modelling work in CLIVAR, which seeks to study the variability and predictability of the climate on seasonal to centennial time scales with the aid of coupled atmosphere-ocean models.

When the Analysis, Interpretation, Modelling and Synthesis (AIMS) phase of WOCE is completed in 2002, the legacy of WOCE will be the successful transfer of a valuable observational and theoretical understanding of the ocean to the other projects of the WCRP, and to CLIVAR in particular. WOCE will also be a challenge to the other WCRP projects to deliver a comparable portrait for the atmospheric/stratospheric, cryospheric, hydrospheric and land surface components of the climate system. On behalf of the JSC I wish to congratulate the WOCE SSG, the WOCE IPO and the many WOCE scientists worldwide for their inspiring vision and for their successful planning, implementation, coordination and documentation of a landmark (or should I say oceanmark) project.

From the WOCE IPO

W. John Gould. john.gould@soc.soton.ac.uk

Breck Owens (SSG co-Chair) and I attended the CLIVAR SSG meeting in Washington DC at the end of April. Their planning is coming along well and an Implementation Strategy (not like the detailed WOCE Plan) is now being developed with some urgency. It seems that many of the key measurements carried out during the WOCE observations will be identified by CLIVAR as central to documenting decadal-scale variability.

WOCE SMWG have completed an Implementation Plan for the AIMS phase and it is now on the desks of about 100 scientists who are being asked to review it before it receives wider circulation this autumn.

As I write this I feel that I am in the middle of a giant cannelloni factory. Sheelagh our secretary is busy putting copies of the WOCE Conference poster in mailing tubes. She and the postman will be glad when they are all on your notice boards! We have the Conference programme virtually complete and the main Conference announcement will be issued in August /September. Please register electronically (http://www.soc.soton.ac.uk/OTHERS/woceipo/wconf) or use the postcard mailed with the last Newsletter.

I'm pleased to have John Church (SSG co-Chair) here in Southampton on a 4-month sabbatical to work on Southern Ocean data and model output. It's good for me to be able to talk to him face-to-face about WOCE without having to negotiate a 10 hr time difference.

The Southern Ocean as the Major Upwelling Zone of North Atlantic Deep Water

Kristofer Döös and Andrew Coward, Southampton Oceanography Centre, UK.
doos@soc.soton.ac.uk

The density difference between the cold and salty water of the North Atlantic and the fresher and warmer waters of the Pacific and Indian Oceans is believed to drive the largest meridional cell in the ocean, known as the Conveyor Belt (Broecker, 1991). The route of the North Atlantic Deep Water (NADW), which is formed by convection at high latitudes, constitutes the deeper branch of the Conveyor Belt. Changes in the movement and characteristics of the NADW are of fundamental importance for understanding our climate, its history and any possible future states (Manabe and Stouffer, 1993; Weaver, 1995). The route and the mechanisms of conversion of the NADW into other water masses are here investigated by following Lagrangian trajectories simulated by a high resolution ocean general circulation model. The traditional view (Stommel, 1958; Robinson and Stommel, 1959) of deep water masses is that they slowly diffuse up evenly through the thermocline at low latitudes. Contrary to this, most of the NADW in the present study is upwelled along the isopycnals in the Southern Ocean and then driven northwards in the surface layer due to the westerlies. In fact only 7% of the NADW eventually upwells in the equatorial regions. The highly eddy active zones, resolved by the model, can also be seen to play an important role in the conversion process.

The ocean general circulation model used in this study is a fully global, high resolution model which has been developed and run by the OCCAM (Webb, 1996) project. Such eddy-resolving models cannot yet be integrated for sufficiently long to reach a dynamic equilibrium state simply because of the huge computer resources required. However, they can be initialised from climatologies of observational temperature and salinity data and integrated forward for sufficient "model years" to spin-up the ocean circulation. Indeed relatively short integrations do have the advantage that the deep ocean circulation will not have "drifted" far from the best available estimate of the state of the real ocean as given by the observational climatologies. The current work is based on the average state of the ocean calculated from model years 8 to 12 of the OCCAM integration.

Improved observational databases, such as those being compiled under the World Ocean Circulation Experiment (Gould and Church, 1996) (WOCE), are unlikely to alter our large-scale view of the ocean circulation. However, they will no doubt contribute significantly to a better description of the ocean, and this in turn will provide a better starting point for investigations into phenomena such as the suspected alternative equilibrium states for the Conveyor Belt (Manabe and Stouffer, 1993; Weaver, 1995) and the potentially dramatic effects these could have on our climate.

Traditionally, water mass studies (Cox, 1985) undertaken with the aid of numerical ocean models have used passive tracers to mark and track the movements of the various water masses. This approach requires the passive tracers to be integrated within the model for, possibly, many model centuries. For high resolution global models this would require computer resources that are unattainable with present technology. The technique utilised in the current study demands considerably less computer resources, and therefore permits (for the first time) the tracing of water masses in high resolution global models. The tracing method (Döös, 1995; Blanke and Raynaud, 1997) involves calculating Lagrangian trajectories from the time-averaged velocity field based on the assumption that each Lagrangian trajectory carries with it a fixed volume. By releasing a very large number of trajectories at different subgrid-scale spatial positions, it becomes possible, for the first time on a global scale, to quantify the transports. In the present study we have followed $15.8 \times 10^6 \mathrm{m}^3/\mathrm{s}$ of NADW by releasing 1.58 million trajectories at the Equator in the Atlantic so that each trajectory carries a mere $10 \mathrm{m}^3/\mathrm{s}$. The number of trajectories released within each model grid cell containing southward flowing NADW is determined by the amplitude of the meridional velocity. The trajectories are released uniformly across the zonal face of the grid cells.

The NADW is followed south from the Equator in the Atlantic until it is converted into a less dense water mass. The usual definition (Emery and Meincke, 1986) of NADW is that water which is denser than $1027.35 \mathrm{kg}/\mathrm{m}^3$ (relative to the surface), however, for the current study, all water denser than $1027.625 \mathrm{kg}/\mathrm{m}^3$ is defined as NADW. This, slightly denser, value was chosen by noting the turning point of the meridional overturning stream function, in isopycnic co-ordinates, at the Equator in the Atlantic. That is to say, water lighter than $1027.625 \mathrm{kg}/\mathrm{m}^3$ has a net northwards transport at the Equator in the Atlantic, whereas denser water has a net southwards component. Thus, by tracking water until it is no longer denser than this value we are able to map out the deeper branch of the Conveyor Belt as it spreads outwards from the equatorial Atlantic to the rest of the world's oceans.

The time (Fig. 1a, page 17) and depth (Fig. 1b, page 17) evolution show how the NADW tends to go into the Antarctic Circumpolar Current, where it either upwells in the Southern Ocean or moves north in the deep ocean into the Indian or Pacific. Most of the water will follow the first route where the water circles in a spiral around Antarctica for a few centuries getting closer to this continent on its way up to the surface. This route corresponds to a ventilated route where the water flows along the isopycnals as long as

it is not in contact with the surface (Luyten et al., 1983; Döös, 1994). The water will, as soon as it arrives in the surface layer, be driven rapidly north by the westerlies and change characteristics due to heat and mass (precipitation and evaporation) exchanges with the atmosphere. The other route, which goes north in the deep ocean corresponds to water that is losing density by mixing with other water masses. The time taken for the NADW to be converted will clearly depend on the route taken. We have found that 71% is converted within the first 250 years, a further 24% is converted over the next 750 years with the remaining 5% taking in excess of 1000 years to reach the lighter density.

A quantification of where the NADW is converted into less dense water can be made by summing the volume transport at the isopycnal $1027.625\,kg/m^3$ for each horizontal model grid cell and then dividing by the area. A NADW upwelling velocity can hence be calculated (Fig. 2, page 17). The major region of upwelling is the Southern Ocean where 9.3 Sv (59%) of the $15.8\times10^6 m^3/s$ of NADW is ventilated along the isopycnals south of 50°S. Most of this is located in the southern part of the Antarctic Circumpolar Current. The second most important region of relatively high vertical velocities of the upwelling NADW is between 36°S and 38.5°S with $1.3\times10^6 m^3/s$ (8%). This is the highly eddy active region of the Agulhas around South Africa where the NADW is converted by mixing with other water masses. The equatorial upwelling is clearly illustrated and is constrained to within a few degrees either side of the equator. The upwelling is only $1.1\times10^6 m^3/s$ (7%) which is rather small compared to the traditional view of strong Equatorial upwelling. The rest of the water is more evenly upwelled over the ocean with stronger upwelling in regions of high eddy activity and western boundary currents. This seems contrary to the traditional view of a uniform upwelling through the thermocline and instead indicates that the upwelling of abyssal water occurs primarily near Antarctica as other recent studies (Toggweiler and Samuels, 1993) indicate.

An important implication of this result is that the details of the ocean circulation in the Southern Ocean may be more important to climate studies than is traditionally considered to be the case. For example, if NADW outcrops south of the westerlies it will not be driven northwards and converted into a lighter water mass. The precise latitude at which the outcropping occurs is strongly dependent on the surface conditions. For ocean-only models, the surface conditions will rely on the quality and coverage of the observational data. For coupled ocean-atmosphere models, they will depend strongly on the ability of the coupled model to simulate correctly the air-sea fluxes.

Acknowledgements

We thank the OCCAM team whose efforts and dedication have made the model integration possible. OCCAM is a NERC funded project which makes extensive use of the UK National supercomputing resource managed and maintained by the Edinburgh Parallel Computing Centre.

Further information can be obtained from http://www.soc.soton.ac.uk/JRD/OCCAM.

References

Blanke, B., and S. Raynaud, 1997: Kinematics of the Pacific Equatorial Undercurrent: A Eulerian and Lagrangian approach from GCM results. J. Phys. Oceanogr., Vol. 27, No. 6, 1038–1053.

Broecker, W. S., 1991: The great ocean conveyor. Oceanography, Vol. 4, No. 2, 79–89.

Cox, M. D., 1985: An eddy resolving numerical model of ventilated thermocline. J. Phys. Oceanogr., 15, 1312–1324.

Döös, K., 1994: Semi-analytical simulation of the meridional cells in the Southern Ocean. J. Phys. Oceanogr., 24, 1281–1293.

Döös, K., 1995: Inter-ocean exchange of water masses. J. Geophys. Res., Vol. 100, No. C7, 13499–13514.

Emery, W. J., and J. Meincke, 1986: Global water masses: summary and review. Oceanologia Acta, 9 (4), 383–391.

Gould, W. J., and J. Church, 1996: Oceans and Climate. Physics World, December, 33–37.

Luyten, J. R., J. Pedlosky and H. Stommel, 1983: The ventilated thermocline. J. Phys. Oceanogr., 13, 292–309.

Manabe, S., and R. J. Stouffer, 1993: Century-scale effects of increased atmosphere CO_2 on the ocean-atmosphere system. Nature, 364, 215–218.

Robinson, A. R., and H. Stommel, 1959: The oceanic thermocline and the associated thermohaline circulation. Tellus, 11, 295–308.

Stommel, H., 1958: The abyssal circulation. Deep-Sea Res., 5, pp. 80-82.

Toggweiler, J. R., and B. Samuels, 1993: New radiocarbon constraints on the upwelling of abyssal water to the ocean's surface. M. Heimann, ed.: The global carbon cycle. NATO ASI Series, Springer-Verlag, Berlin, 333–366.

Weaver, A. J., 1995: Driving the ocean conveyor. Nature, 378, 135–136.

Webb, D. J., 1996: An ocean model code for array processor computers. Computers and Geosciences, 5, 569–578.

ERRATA CORRIGE

To those of you who noticed the printing error in the previous Newsletter issue, No. 26, page 3, second column, first line of the Peter Baines' article "Some Oceanographic Inferences from Coarse-Resolution Ocean and Climate Models", the line should read:

<<was first noticed by Gill and Bryan (1971). The magnitude>>

Many apologies for any inconvenience that this might have caused.

Eddy Statistics Reveal Currents in the Southern Ocean

Chris W. Hughes, Proudman Oceanographic Laboratory, Birkenhead, L43 7RA, UK; Matt S. Jones, James Rennell Division, Southampton Oceanography Centre, Southampton SO14 3ZH, UK; and Stuart Carnochan, Dept. of Civil Engineering, University of Aston, Birmingham B4 7ET, UK. C.Hughes@pol.ac.uk

Background

The dynamics of the Southern Ocean are unique in that interactions with bottom topography are necessary to balance the angular momentum budget at the latitudes of Drake Passage. At other latitudes, the torque exerted by wind stress can be balanced by a pressure torque on the continents, but it is now generally accepted that the angular momentum input by wind stress in the Southern Ocean is somehow transferred to the deep ocean, where it is removed by a pressure torque on the bottom topography.

Another way to look at this is in terms of a meridional overturning. The eastward wind stress is balanced at the surface by the Coriolis force, producing northward flow in the Ekman layer. To close the mass budget, this northward flow must return southwards at depth. If the return flow across a latitude line is to be geostrophic, then it must occur 'leaning up' against the bottom topography, since the total transport through a zonal section is proportional to the pressure difference across that section. When the section passes right round the earth, the 'ends' of the section are in the same place, with the same value of pressure, and hence no net transport. In order for a net transport to occur at some depth, the section must be interrupted by bottom topography, with a pressure difference across the bottom topography.

The question then is, how does this overturning circulation come about? A mechanism must be found which does not rely on a fortuitous balance between the strengths of the wind forcing and the thermohaline circulation. Döös and Webb (1994) have outlined such a mechanism, which explains the Deacon Cell as modelled in the Fine Resolution Antarctic Model (FRAM). This mechanism requires a current which penetrates to sufficient depth to interact with the bottom topography, as the Antarctic Circumpolar Current (ACC) is known to do.

There is a dynamical problem here though. In wind-driven spin-up experiments, Anderson and Killworth (1977) showed that baroclinic Rossby waves act to shut off the deep circulation, insulating the ocean from any kind of interaction with the bottom topography. This is why the Sverdrup balance is so successful in describing the subtropical ocean gyres. Why does this not happen in the Southern Ocean? The answer lies in the mean flow. In fact, if mean flows are ignored completely, linear theory predicts that a series of Rossby waves, of higher and higher vertical mode number, would traverse the ocean basins confining the wind driven circulation to an ever thinner layer at the surface. This process is actually halted when the mean flow becomes fast enough to influence the propagation of Rossby waves of some vertical mode number, so higher order modes can produce no further thinning. In the Southern Ocean, where the flow must interact with topography, the first (fastest) baroclinic mode must be overwhelmed by the mean flow. To be precise, it is the long, first baroclinic mode which must be overwhelmed, and since this is the fastest that means that the mean flow must be strong enough to advect all baroclinic waves eastwards.

This behaviour has been observed in FRAM (Hughes, 1996), and leads to some interesting dynamics. Rossby waves tend to diffract out of an eastward flow, but eastward-travelling waves cannot exist outside the eastward flow. This apparent contradiction leads to the occurence of a critical layer, where waves break (in the horizontal plane), and strong wave/mean-flow interactions occur. Such processes have been shown to have a profound impact on mixing in stratospheric dynamics.

Data and analysis

To determine whether similar dynamics are occurring in the real Southern Ocean is more difficult. Hughes (1995) used TOPEX/POSEIDON (T/P) altimetry to show that there are regions of eastward and westward propagation of wavelike disturbances in the southeast Pacific, but only a small region could be mapped because the wavelengths (typically 250 km) are comparable to the cross-track spacing of the T/P altimeters. Here, two data sources with higher spatial resolution are employed. The 35 day repeat phase of the ERS-1 altimeter has a cross-track separation of 360/501=0.72 degrees of longitude, or about 50 km at a latitude of 50°S. The ERS-1 orbits were improved by use of dual crossovers with T/P altimetry (Carnochan, 1996), and the effect of long wavelength error was minimised by considering the along-track gradient. The high inclination of the ERS-1 orbit means that, for practical purposes, the along-track gradient is virtually a measure of the zonal geostrophic current, and that is how it is used here (tests with FRAM and the temperature data described below show that this is a good approximation). There are 18 cycles of the 35 day repeat phase, and the use of both ascending and descending tracks at crossover points means that there are, at most, 36 measurements at each point.

A sea surface temperature dataset measured by the Along-Track Scanning Radiometer (ATSR) is available at half degree resolution. Here, zonal gradients of sea surface temperature (SST) are considered, using monthly median values of SST calculated after rejection of values contaminated by marine stratiform cloud (Jones et al., 1996a, b). It is not obvious that SSTs will reflect the geostrophic currents. However, the atmospheric forcing which would tend to destroy the relationship between SSTs and currents is typically on length scales larger than 1000 km,

so the SST gradients should be related to currents on scales smaller than this. The data set includes 44 months of SST measurements, although obscuration by clouds means there are few places where there are good measurements for all 44 months.

Using these two datasets, cross spectra were calculated between time series at one grid point and at the next grid point to the east (in fact, the cross spectra were calculated from auto- and cross-covariances from a zonally orientated patch of 9 grid points, assuming homogeneous statistics over this area. This seems to give a good balance between spatial resolution and errors). The cross spectra define a phase lag between one grid point and the next for each frequency, and from this a wavenumber can be calculated. The short lengths of the altimetric and SST time series mean that spectral resolution is quite poor, but this should not lead to problems in defining propagation direction if the waves are either all travelling eastwards or all travelling westwards. Examination of wavenumbers for different wave periods shows that this tends to be the case.

Results

Fig. 1 (page 18) shows wavenumbers from the altimetry (at a period of 4.6 months), and from ATSR zonal temperature gradients (at 4.8 months). Superimposed on these figures are mean SST contours from ATSR. It is quite clear that the strong eastward flow in the ACC is advecting disturbances eastwards, whereas westward propagation predominates in the slower currents further north, as would be expected for normal Rossby waves. The directions shown by ATSR and altimeter are in excellent agreement. Apart from the broad region of eastward propagation in the ACC, there are some interesting smaller features, most clearly visible in the higher resolution ATSR data. There is a region of eastward propagation to the northwest of New Zealand, where a strong eastward current is known to flow in the Tasman Front. Eastward propagation in the South Atlantic Current (about 38°S, 10°W) is separated from the ACC by a clear band of westward propagation. Another interesting feature is what appears to be eastward propagation along a line southwest of Madagascar. This is also clear in FRAM and OCCAM (Ocean Circulation and Climate Advanced Modelling) data, where it corresponds to a strong westward current. Further investigation is needed to see whether this is due to aliasing of a fast westward propagation.

The propagation directions in Fig. 1 are robust, but the wavenumber values are quite sensitive to details of the analysis. These values are affected by parameters used for spectral analysis, the grid point spacing used, and the direction of the sea surface gradient or SST gradient used. One result which is robust is that the wavenumbers calculated from meridional gradients (corresponding to zonal currents) are smaller than those calculated from zonal gradients by a factor of about 2 or 3. This holds for ATSR and FRAM SSTs, and FRAM sea surface slopes, though it cannot be tested with ERS-1 altimetric slopes. It is clear from these sensitivities that the spectra are not simple, and there is potentially much more information to be extracted from the spectra and cross spectra than simply propagation direction. Given the success of propagation direction in reflecting important aspects of the mean flow, investigation of other aspects of the spectral information seems likely to be profitable.

References

Anderson, D. L. T., and P. D. Killworth, 1977: Spin-up of a stratified ocean, with topography. Deep-Sea Res., 24, 709–732.

Carnochan, S., 1996: Orbit and Altimeter Corrections for the ERS Satellites Through Analysis of Single and Dual Satellite Crossovers, Ph.D. thesis (submitted), Aston University, Birmingham.

Döös, K., and D. J. Webb, 1994: The Deacon cell and other meridional cells of the Southern Ocean. J. Phys. Oceanogr., 24, 429–442.

Hughes, C. W., 1995: Rossby Waves in the Southern Ocean: A Comparison of TOPEX/POSEIDON Altimetry with Model Predictions. J. Geophys. Res., 100, 15933–15950.

Hughes, C. W., 1996: The Antarctic Circumpolar Current as a Waveguide for Rossby Waves. J. Phys. Oceanogr, 26, 1375–1387.

Jones, M. S., M. A. Saunders, and T. H. Guymer, 1996: Reducing cloud contamination in ATSR averaged sea surface temperature data. J. Atmos. Oceanic Tech., 213, 492–506.

Jones, M. S., M. A. Saunders, and T. H. Guymer, 1996: Global remnanat cloud contamination in the along-track scanning radiometer data: Source and removal. J. Geophys. Res., 101, 12141–12147.

New Pages at the WOCE-IPO Web Site

In conjunction with the WOCE workshops on the South Atlantic (Brest, 16–20 June) and on the Southern Ocean (Hobart, 8–12 July), the IPO has posted a collection of references appropriate to each area

(http://www.soc.soton.ac.uk/OTHERS/woceipo/satlbib.html,
http://www.soc.soton.ac.uk/OTHERS/woceipo/antbib.html).

The references were selected by Jim Crease at the DIU from the WOCE bibliography using the keywords which accompany each entry: the bibliography now contains over 2000 references

(http://diu.cms.udel.edu/woce/woce_bib.html).

Also recently added are pages containing information about the WOCE Conference (Halifax, 24–29 May 1998)

(http://www.soc.soton.ac.uk/OTHERS/woceipo/wconf)

which includes the draft programme for the conference.

A Steady State Inverse Model of the Large Scale Circulation in the Argentine Basin

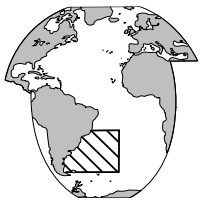

Véronique C. Garçon and L. Larqué, UMR5566, CNRS/CNES/Université, Toulouse, France; K. Maamaatuaiahutapu, University of the South Pacific, Suva, Fiji; and C. Provost, LODYC, CNRS/ORSTOM/Université, Paris, France. garcon@pontos.cst.cnes.fr

Introduction

The South Atlantic witnesses a wide range of flow regimes, ranging from small-scale transient eddy flows (Agulhas outflow and Brazil/Malvinas Confluence) to the large-scale recirculation of the world ocean's dominant deep water mass (North Atlantic Deep Water (NADW)). The Brazil-Malvinas Confluence is identified as the encounter around 38°S, of the poleward-flowing Brazil Current (BC) and of the equatorward-flowing Malvinas Current (MC) along the western margin of the Argentine basin. The WOCE Confluence programme is a joint effort between the US, France and Argentina to provide a high-resolution picture of the dynamics of the Brazil/Malvinas Confluence region (Confluence Group, 1990). Among the various objectives of the programme, one is to provide estimates of the transports of mass and tracers in the western boundary currents in each water mass and to assess the importance of the recirculation in the Argentine basin. Maamaatuaiahutapu et al. (1992) showed, using data from the various Confluence cruises in the region and a multiparameter analysis of water mass composition, that local recirculation of Antarctic Intermediate Water (AAIW) is largely influenced by the two strong currents, Brazil and Malvinas.

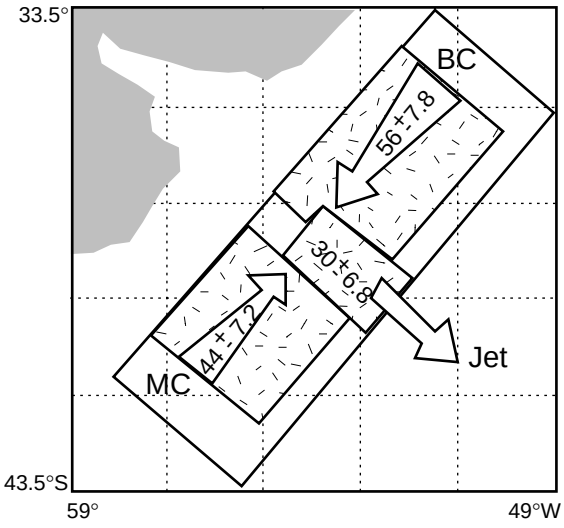

Figure 1. Depth integrated transports of the Brazil, Malvinas currents and the jet based on inversion of the Confluence 3 data set. The transports are averaged from 7 and 6 sections to compute the Brazil and Malvinas transports, respectively corresponding to each current region. For the jet, according to the bottom depth and the water layer, 5 to 8 sections are included.

Maamaatuaiahutapu et al. (1997) used data from the Confluence 3 cruise, collected in the area 35°–42°S, 50°–58° W, mainly over the continental slope and shelf and a nonlinear inverse model to provide total geostrophic transports estimates of the MC and BC. They found 44±7 Sv and 56±8 Sv for the MC and BC, respectively (Fig. 1). Due to the recirculation cells within the Argentine Basin, we choose to extend our area of study eastwards within the Argentine Basin to provide as robust an estimate as possible of the volume transports of these two boundary currents.

Data and analysis

The data set used in this analysis consists of historical hydrographic CTD observations measured at discrete depths in the 30°–60°S and 20°–70°W domain over the last eighty years, some of which have been already assembled in atlases (Reid, 1981; Gordon and Molinelli, 1982; Mantyla and Reid, 1983; Charo et al., 1991; Provost et al., 1991; Kartavtseff et al., 1994; Reynaud, pers. com.). Of the 8234 stations thus collected, 5026 were selected after careful individual examination. Criteria for selection were twofold: a reasonable data density down to the bottom and no inconsistent variability (Larqué, 1996). Because of the computational time of the inversion, the vertical resolution is reduced and only 38 depths levels are used (5, 10 m, every 10 m for the first 100 m, 150, 200 m, every 100 m down to 1000 m and every 250 m for the 1000–5000 m interval). In order to further decrease the amount of data, vertical empirical orthogonal functions of the temperature, salinity and density fields were calculated using a singular value decomposition of the vertical covariance matrices. Horizontal coefficients are then obtained by projecting the original data onto the EOFs. Ten functions are shown to be sufficient for a correct reconstruction of the property fields (Larqué, 1996). The EOF coefficients were then interpolated onto the regular grid shown in Fig. 2 (page 19) using an objective analysis procedure. The grid resolution is 1° by 1° degree in both directions. A sum of four isotropic Gaussian functions with correlation length scales of 250, 500, 1000, and 2000 km is taken as the spatial correlation function. The in situ density fields reconstructed with the first 10 EOFs after objective interpolation of its coefficients at the model grid points describe fairly well our present knowledge of the circulation in the Argentine basin.

The purpose of the nonlinear inverse model we used (Mercier, 1986) is to search for horizontal reference velocities and density fields at model grid points as close as possible from the density data while satisfying the dynamical constraints. Constraints include Ekman constraints,

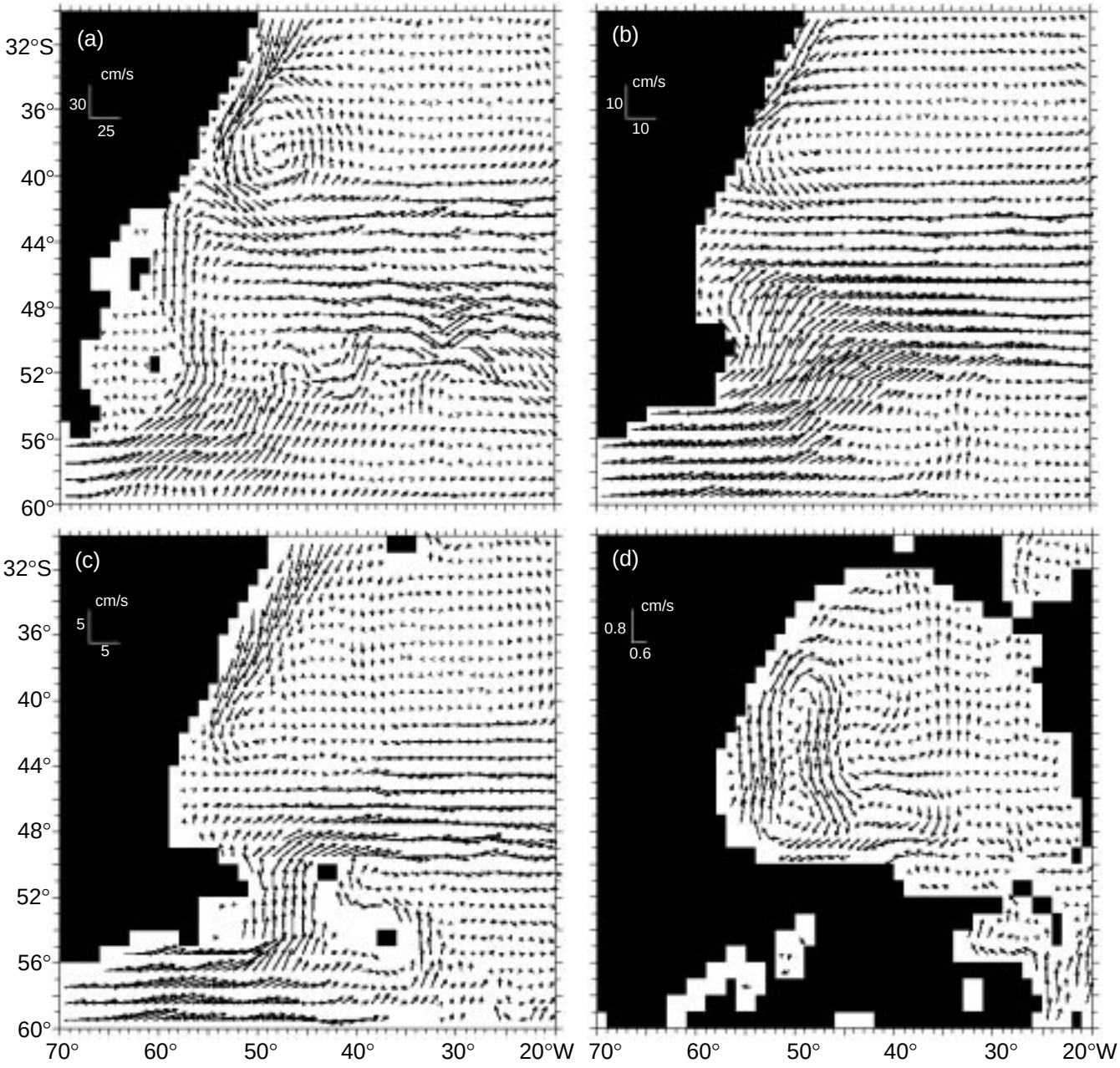

Figure 3. Steady state velocity field (cm/s) at (a) 100 m, (b) 900 m, (c) 2500 m and (d) 4250 m after inversion.

conservation constraints (mass, planetary vorticity, heat and salt) and two integrated transport constraints, one meridional at Drake passage (130±40 Sv) at the south-western boundary of the domain (56.5°–59.5°S) and one zonal at the Brazil Current inflow in our northwestern domain boundary at 30.5°S (40±20 Sv). Covariance matrices associated to each constraint type are detailed in Larqué (1996).

Results

Several inversion experiments were performed using different levels of no motion and surface wind stress sources. We also examined the effect of introducing the two integrated transport constraints mentioned above. Fig. 3 shows a few model results in the case of the inversion with a reference level chosen at 3000 m, a climatological mean sea surface wind stress from ECMWF over the years 1986 to 1988, and with the transport constraints.

The steady state velocity field at 100 m (Fig. 3a) exhibits an intensification of the BC until 38.5°S with maximum velocity values of 28 cm/s; at the surface they can reach 42 cm/s. A recirculation loop of the BC between 35°–41°S and 52°–41°W is present corroborating some 3D modelling studies results. The subtropical front exits the domain at 41.5°–42.5°S with a jet velocity reaching 16 cm/s at 100 m and 24 cm/s at the surface. The subantarctic and polar fronts are quite indistinguishable, eastward surface currents have mean values of 26 cm/s. The MC is well marked, flowing adjacent to the coast with maximal values

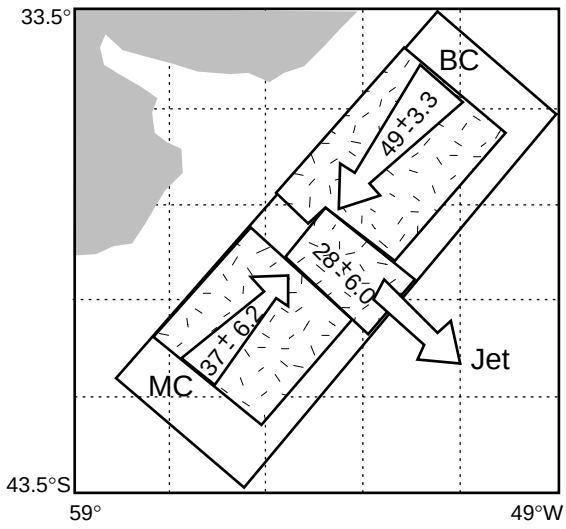

Figure 4. Depth-integrated transports of the Brazil, Malvinas currents and the jet based on inversion of the historical data set.

of 26 cm/s at 100 m and 31 cm/s at the surface. It encounters the BC at around 39°–40°S from which point the two currents merge and turn eastward to enter the Antarctic Circumpolar Current (ACC).

Fig. 3b shows in the north of our domain at 900 m depth the horizontal ocean current squeezed along the slope and underlying the surface BC. Velocity is 9.7 cm/s at 30.5°S and 12 cm/s at 35.°S. A recirculation loop of Antarctic intermediate waters occurs between 31.5° and 36.5°S and encounter of both western boundary currents occurs around 42°S. AAIW then turns eastward as part of the subtropical gyre undergoing a recirculation within the Argentine basin itself. Along 34.5°W, south of 53.5°S, a branch of the ACC originating from the polar front appears clearly. The AAIW spreading path shows no evidence of a primary route along the western boundary in the Argentine basin.

The convergence between the deep western boundary current flowing poleward and the equatorward circumpolar deep waters occurs between 43.5°–46.5°S (Fig. 3c). The poleward current velocity at 2500 m depth may reach values up to 6 cm/s. NADW recirculation within the Argentine basin is clearly visible. At the Río Grande Seamounts passage (RGS) (31°S, 35°W), an eastern branch appears at 33.5°S forming the western branch of a recirculation gyre centred at 30°W–36°S. The northern branch of this gyre splits in two parts, one remains south of the RGS and the other proceeds around them northward. Circumpolar Deep Water (CDW) enters the Argentine basin west and east of the Ewing Bank (53°S, 40°W).

At 4250 m depth (Fig. 3d), the Weddell Sea Deep Water (WSDW) performs a recirculation loop centred along the 49.5°W axis, following the 5500 m isobath and extending eastward until 33.5°W between 45.5°–48.5°S. One can note the separation of this loop at 37.5°S in two branches: one deviates towards the north and flows towards the RGS in the Vema Channel (west of RGS) and Hunter Channel (east of RGS), the southern one finally joins the main loop at 42°S. East of the Ewing Bank, WSDW exits the basin eastward. In the Georgia basin (54°S, 35°W), the current is confined in the west and then enters the Argentine basin. The existence of the Zapiola anticyclone around the depositional feature known as the Zapiola Drift (45°S, 40°W) seems to be confirmed. Indeed one can observe westward velocities on the northern flank of the Drift at 42°–43°S, whereas south of the Drift, at 46°S, the current has a mostly eastward component. On the western and eastern flanks of the ridge, southgoing (along 47°W) and northgoing (along 36°W) currents are detected.

Finally, estimates of integrated transports of the BC, MC and the resulting jet in the Confluence area yield the following values: 49.2±3.3 Sv, 36.9±6.2 Sv, 28.2±6 Sv, respectively (Fig. 4). In the upper warm water sphere (down to 800 m), the BC and MC carry 29.6±7.1 Sv, and 25.3±3.8 Sv, respectively.

Summary

By extending our domain geographically within the Argentine basin, we are able to provide transport estimates of the BC and MC in the Confluence area, equal to 49±3 Sv and 37±6 Sv, respectively, including all recirculation cells. Those numbers are slightly lower than those of Maamaatuaiahutapu et al. (1997). Indeed our estimates correspond to a steady state oceanic circulation where interannual variability has been smoothed out. It is shown that the flow pathway of the AAIW does not favour the western boundary passage between 40°–20°S in the Argentine basin. The circulation scheme of NADW around the RGS is refined. Our inversion results seem to confirm the existence of an anticyclonic flow around the Zapiola Drift at the abyssal levels.

Acknowledgements

This work was supported by a grant of the Centre National de la Recherche Scientifique (PNEDC:WOCE) to UMR5566 and LODYC. We wish to thank Pascal Legrand for assistance with the nonlinear inversion code and Thierry Reynaud for providing us with hydrographic CTD observations.

References

Charo, M., A-P. Osiroff, A. Bianchi, and A. Piola, 1991: Datos fisicos, chimicos, CTD y XBT. Campañas oceanograficas Puerto Deseado 02-88, Confluencia 88 y 89, Inf. Tech., 59/1991, SHN, Buenos Aires, 422pp.

Confluence Group, 1990: Confluence 1988–1990, An Intensive study of the southwestern Atlantic. EOS, 71(41), 1131–1137.

Gordon, A. L., and E. J. Molinelli, 1982: Southern Ocean Atlas. Columbia University Press, New York.

Kartavtseff, A., E. Kestenare, and C. Provost, 1994: Données CDT-O2. Internal Report LODYC, No 94/03, 231pp.

Larqué, L., 1996: Etude des masses d'eau en Atlantique Sud et de la circulation océanique à grande échelle dans le bassin argentin. PhD thesis, University Paul Sabatier, Toulouse, France, 168pp.

Maamaatuaiahutapu, K., V. Garçon, C. Provost, M. Boulahdid, and A-P. Osiroff, 1992: Brazil/Malvinas Confluence: Water

mass composition. J. Geophys. Res., 97(C6), 9493–9505.
Maamaatuaiahutapu, K., V. Garçon, C. Provost, and H. Mercier, 1997: Transports of the Brazil and Malvinas Currents at their Confluence. J. Mar. Res, in revision.
Mantyla, A. W., and J. L. Reid, 1983: Abyssal characteristics of the World Ocean waters. Deep-Sea Res., 30, 8A, 805–833.
Mercier, H., 1986: Determining the general circulation of the ocean: a nonlinear inverse problem. J. Geophys. Res., 91, 5103–5109.
Provost, C., L. Mémery, and B. Torres Lista, 1991: Données CTD-O_2. Internal Report LODYC, No. 91/02, 188pp.
Reid, J. L., 1981: On the mid-depth circulation of the world ocean. In: Evolution of Physical Oceanography, B. Warren and C. Wunsch, Eds., MIT Press, 70–111.

AR8: Upper Ocean Variability and Mixing in the Brazil Malvinas Confluence

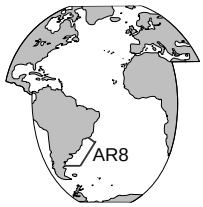

A. A. Bianchi, A. R. Piola, A. P. Osiroff and M. Charo, Servicio de Hidrografia Naval, Montes de Oca 2124, (1271) Buenos Aires, Argentina. abianchi@oceanar.mil.ar

Introduction

The most prominent feature of the upper circulation of the Western South Atlantic is the encounter of two boundary currents at the Brazil/Malvinas Confluence (BMC) in the area of the Argentine Basin. The area is referred as to AR8 of the WOCE Hydrographic Programme (WHP). The Malvinas Current originates as a branch of the Antarctic Circumpolar Current downstream of the Drake Passage and flows northward into the Argentine Basin along its western boundary. The Brazil Current flows poleward along the continental slope of South America. Between 35° and 39°S, this current converges with the Malvinas Current causing a sharp thermohaline front (Roden, 1986, Gordon, 1989).

The BMC is marked by the high meso-scale variability evident from hydrographic data, infra-red imagery (Olson et al., 1988), satellite-tracked surface drifters (Piola et al., 1987) and altimetry (Zlotnicki and Fu, 1989).

In order to determine the space-time scales and the intensity of variability in AR8 region and possible water mass exchanges between Brazil and Argentine Basins (two major objectives of WHP and Deep Basin Experiment), repeated surveys are required to examine interannual signals in the temperature and salinity fields.

Field activity

From 1988 to 1995, 12 hydrographic cruises took place in the region of the BMC in the Western South Atlantic (Fig. 1). All cruises were a follow-up of the pre-WOCE project Confluence (an international cooperative programme between USA-France-Argentina, Confluence Principal Investigators, 1990) and the Southwestern Atlantic Boundary Currents (1991 to present) which we are reporting in this article. In all the cruises CTD profiles were taken and temperature and salinity observations were made and records from an array of 10 inverted echo-sounders were obtained from November of 1988 to February 1990 (Garzoli, 1993). In addition dissolved oxygen, nitrates, silicate and phosphate samples were measured in some cruises, and ancillary biological sampling programmes were carried out in most cruises. More than 20 synoptic sections of the front were obtained; most of the sections were occupied at 39°S of latitude.

The objectives of the repeated surveys are:

- To determine the space-time scales of the variability.
- Quantify the cross-front property (heat, salt) transfer

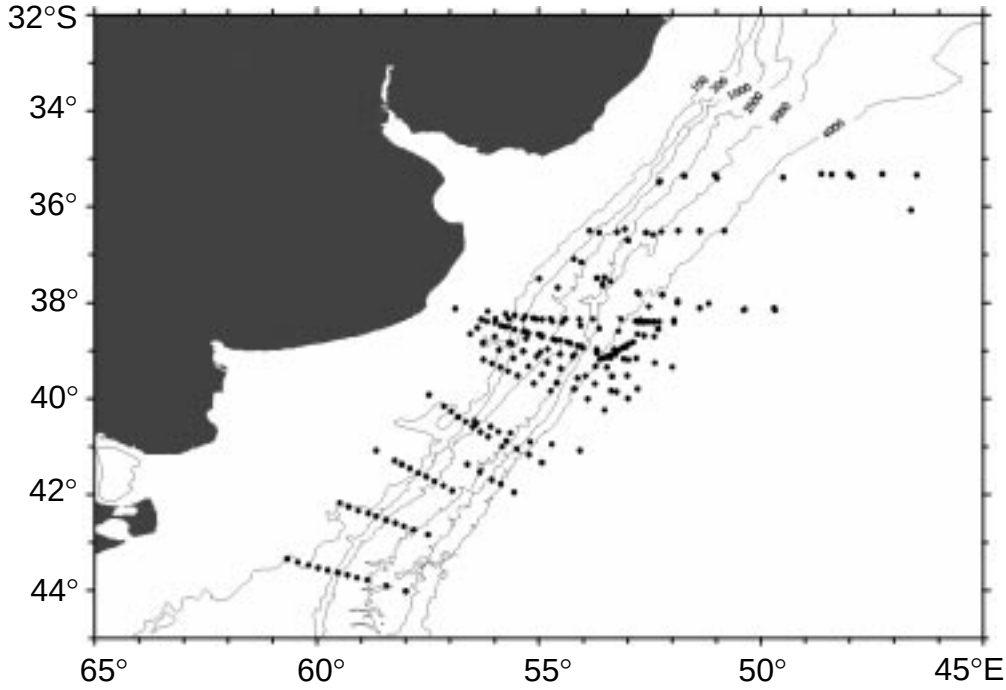

Figure 1. Position of CTD stations occupied in 12 oceanographic cruises taken in WOCE region AR8 between 1988 and 1995.

due to meso-scale processes.

- Study the regional dynamics that cause the observed variability.
- Identify features of the front that may have impact on large scales patterns of global circulation.

Based on this data-set, cross-frontal property fluxes were estimated (Bianchi et al., 1993), space-time scales and ranges of different frontal parameters were determined and geostrophic transports of the upper ocean have been calculated (Piola et al., in preparation). The main results of these studies are outlined in this note.

Results

The mean values of upper ocean cross-front temperature and salinity gradients of order 10^{-4}°C / m and 10^{-5} psu / m were estimated (Fig. 2, page 19). High-resolution surveys (Piola and Bianchi, 1992) reveal that cross-front gradients may be as high as 3°C/km and 0.25 psu/km at 200 m depth. Cross-front differences in the vertically averaged temperature and salinity of the upper 500 m across the front are 10.6°C (within a range of 10.0 to 11.5°C) and 1.4 psu (within a range of 1.2 to 1.6). Frontal displacements in the meridional direction exceed 200 km in 15 days and the distances from the front to the continental slope vary from 60 to 260 km.

Based on a statistical model (Joyce, 1977), medium scale cross-frontal heat and salt fluxes were estimated as a function of variances of the vertical property gradients in a 10 to 100 m wavelength band and the mean values of the horizontal property gradient in the frontal region. Results indicate that mixing is a very effective mechanism in dissipation of eddies and intrusive lenses across the front (Bianchi et al., 1993). Estimated fluxes of heat (10^{-2}°C m / s) and salt (10^{-3} psu m / s) are the highest in the world ocean (an order of magnitude higher than other available estimates for frontal regions). Extrapolation of these fluxes to the South Atlantic Subtropical Convergence from South America to Africa, suggest that 20 to 50% of poleward large-scale heat flux and 20% of the excess of evaporation over precipitation north of 30°S can be balanced by these cross-frontal fluxes. Thus, the frontal interleaving may play a key role on Atlantic heat and freshwater budgets.

Another finestructure signature of the BMC is the step-like structure of the temperature and salinity profiles in the front at thermocline levels. This feature is believed to be related to salt-fingering or double diffusion activity at the interface between warm and salty water over cold and fresh water (Schmitt, 1981). The interface is produced in the South Western Atlantic between the Subtropical Water and the Antarctic Intermediate Water (AAIW). Using the model of Kunze (1987) on these "steps" leads to averaged salt fluxes due to salt-fingers of 3.5×10^{-7} psu m / s (Bianchi and Collino, in preparation). These values are of the same order of magnitude of the estimated fluxes on meddies in the Eastern North Atlantic, close to the Gibraltar Strait (Hebert, 1988). In addition, in winter the vertical salinity is further increased due to enhanced evaporation. Thus, a large vertical salt flux occurs in the Western South Atlantic, associated to the high vertical salinity gradient across the pycnocline. Both processes, convection and salt-fingers, sustain the thermocline ventilation hypothesis of Gordon (1981). Estimates of salt fluxes in these thermohaline staircases suggest that the mixing rate of salt is an order of magnitude larger than in other areas (Schmitt, 1995). These processes may provide a critical vertical path for salt, oxygen and nutrients.

Annual and semi-annual signals have been identified as an important source of variability in this region (Olson et al., 1988). However, large amplitude meridional and zonal frontal motions not apparently related with any seasonal pattern were detected (Bianchi and Garzoli, 1996). The meridional displacements of the front have average velocities of 0.2 m/s. Some of these displacements have been linked with intensification of cyclonic wind circulation southward of the area (Garzoli and Giulivi, 1994). Further investigation of Antarctic Circumpolar Current transport variability and its possible relation with Malvinas Current intensification is required. The annual cycle of southward geostrophic transport estimates related to 1000 dbars are presented in Fig. 3 (Piola et al., in preparation) between 32°S and 40°S of latitude. The variability range is of the same order of the mean value and no seasonal pattern are apparent. Because not all the sections were strictly normal to the front it is difficult to assess the transport variability. The annual and semi annual cycles of the BMC are not the only nor the most important source of variability and future work is required to better understand the transport fluctuations.

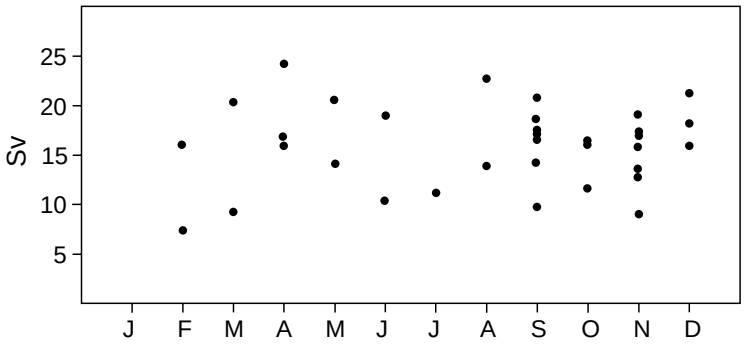

Figure 3. Annual cycle of geostrophic southward transport referred to 1000 dbar using historical synoptic sections of the front between 32° and 40°S. The variability and the mean transport are of the same order of magnitude, and seasonality is not apparent.

Acknowledgements

We acknowledge the scientists and crew members that participated in the different WOCE AR8 hydrographic cruises. The work reported here was financed by Servicio de Hidrografia Naval, Argentina.

References

Bianchi, A. A., y Collino (in preparation), Difusion doble y mezcla en el Atlantico Sudoccidental.
Bianchi, A. A. and S. L. Garzoli, 1996: Variability and Motion in the Brazil-Malvinas Confluence. Geoacta, in press.
Bianchi, A. A., C. F. Giulivi and A. R. Piola, 1993: Mixing in the Brazil-Malvinas Confluence. Deep-Sea Res., I, 40, 1345–1358.
Garzoli, S. L., 1993: Geostrophic Velocity and Transport Variability in the Brasil/Malvinas Confluence. Deep-Sea Res., 40, 1379–1404.
Garzoli, S. L., and C. F. Giulivi, 1994: What Forces the Variability of the South Western Atlantic Boundary Currents? Deep-Sea Res., 41, 1527–1550.
Gordon, A. L., 1981: South Atlantic Thermocline Ventilation. Deep-Sea Res., 28, 1239–1264.
Gordon A. L., 1989: Brazil-Malvinas Confluence-1984. Deep-Sea Res., 36, 359–384.
Hebert, D., 1998: Estimates of salt-finger fluxes. Deep-Sea Res., 35, 1887, 1901.
Joyce, T., 1977: A note on the lateral mixing of water masses. J. Phys. Oceanogr., 7, 626–629.
Kunze, E., 1987: Limits on growing, finite-length salt fingers: a Richardson number constraint. J. Mar. Res., 29, 375–401.
Olson, D., G. Podesta, R. H. Evans, and O. Brown, 1988: Temporal variations in the separation of Brazil and Malvinas Currents. Deep-Sea Res., 35, 1971–1990.
Piola, A. R., and A. A. Bianchi, 1992: AR8: Southwest Atlantic Boundary Currents. Int. WOCE Newsletter No. 12, pp 14–16.
Piola, A. R., H. A. Figueroa, and A. A. Bianchi, 1987: Some aspects of the surface circulation South of 20°S revealed by First GARP Global Experiment Drifters. J. Geophys. Res., 92, 5101–5114.
Piola, A. R., A. P. Osiroff, and A. A. Bianchi. Upper ocean physical oceanography of the Western South Atlantic, in preparation.
Roden, G. I., 1986: Thermohaline fronts and baroclinic flow in the Argentine Basin during the Austral Spring of 1984. J. Geophys. Res., 91, 5075–5093.
Schmitt, R. W., 1981: Form of the Temperature-Salinity Relationship in the central water. Evidence for Double-Diffusive Mixing. J. Phys. Oceanogr., 11, 1015-1025.
Schmitt, R., 1995: The Ocean's Salt Fingers. Scientific American, 272, 5, 50–55.
Zlotnicki, V., and L. L. Fu, 1990: Seasonal Variability in Global Sea level Observed with Geosat Altimetry. J. Geophys. Res., 94, 17959–17971.

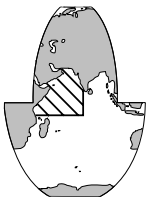

Tracer Distributions in the Arabian Sea, 1995

Monika Rhein, Olaf Plähn, and Lothar Stramma, Institut für Meereskunde an der Universität Kiel, 24105 Kiel, Germany. mrhein@ifm.uni-kiel.de

Introduction

As part of the German WOCE efforts, an extensive observational programme was carried out in the Arabian Sea, March–September 1995 (Fig. 1). The programme included a moored current meter array and shipboard observations of water masses ($CTD-O_2$ and chlorofluorocarbons CFC-11 and CFC-12) as well as direct velocity measurements with shipboard and lowered ADCP and Pegasus (Schott et al., 1997). Tracer measurements were taken in March–April, the intermonsoon period, in June–July at the height of the southwest monsoon, and during the late phase of the monsoon in mid August–September 1995. The main objectives of the tracer measurements were to study the influence of the monsoon on the gas saturations of the upper layer and to analyse the tracer signals of the intermediate water masses (Rhein et al., 1997). In total, about 3000 CFC samples were analysed, the accuracy varied from ±1.0 to 1.3% for the three cruises. CFC-11 data were only available from the cruises M32/4 and M32/6 (Fig. 1). In the Arabian Sea, no deep and bottom water masses are formed, and the CFC signals of the Antarctic Bottom Water and North Atlantic Deep Water have not reached the region yet. Thus, the CFC concentrations below 1000–1200 m depth were below detection limit. Outside the Gulf of Oman and the Gulf of Aden, CFCs decrease almost exponentially with depth (Fig. 2). The temporal changes in the upper 700 m are caused by the response of the Indian Ocean to the monsoon and air-sea gas exchange. The CFC surface concentrations in the Arabian Sea are about 1 pmol/kg CFC-12 and 2 pmol/kg CFC-11. Due to the temperature dependence of solubility (Warner and Weiss, 1985), these values are much lower than observed in high latitude regions.

Surface saturations

Spatial and temporal variability of the CFC saturations are entirely caused by physical processes. Disequilibrium occurs, for instance, through cooling/warming of the sea surface, through upwelling or deepening of the mixed

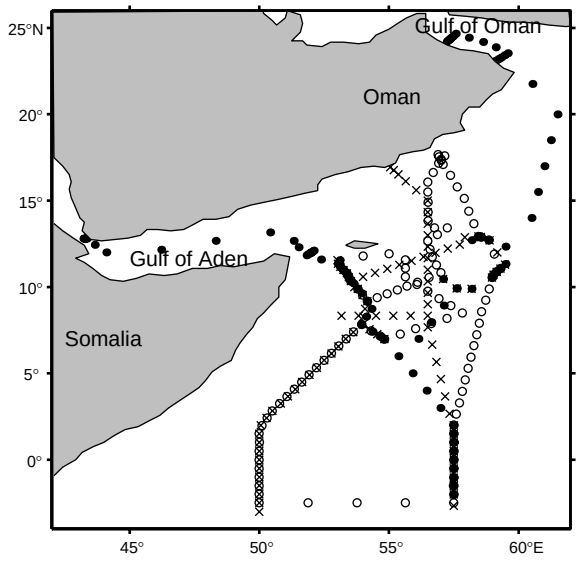

Figure 1. Station map, RV Meteor cruises M32/1, March–April 1995 (black dots); M32/4, June–July 1995 (crosses); and M32/6, August–September 1995 (open circles).

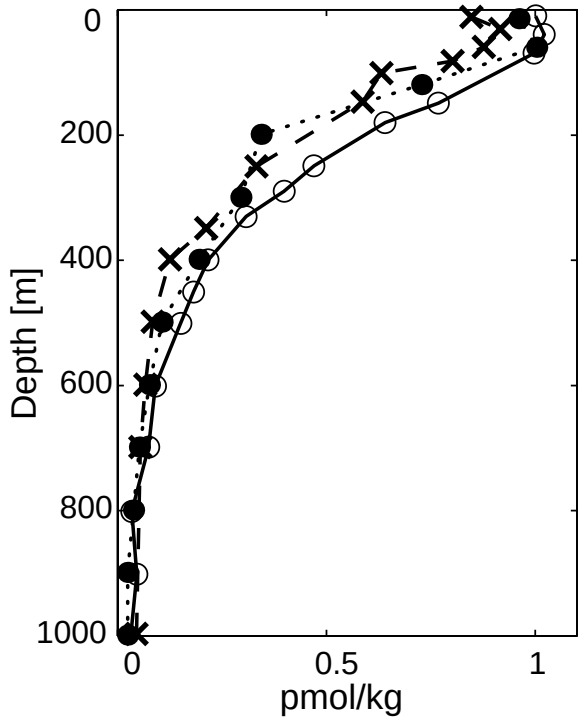

Figure 2. CFC-12 profiles at 10°N, 56°E, measured in March (black dots), June 1995 (crosses) and September 1995 (open circles).

layer, entraining CFC-poorer water to the surface. The intensity of the saturation decrease due to mixed layer deepening is dependent on the vertical structure of the CFC profile. Air-sea gas exchange, which is mainly a function of wind speed, restores the equilibrium, but is often too slow to do that instantaneously.

During the intermonsoonal period (March–April 1995), the surface waters were supersaturated with respect to the CFCs, caused by a combination of warming at the surface and slow gas exchange due to small wind speeds during that period (Fig. 3a). The observed saturations are comparable to model results of Haine et al. (1997). With the beginning of the summer monsoon the CFC surface saturations decreased due to the deepening of the mixed layer and due to upwelling near the coast. The lowest saturations (70%) were observed in the upwelling region near the coast of Oman (Fig. 3b). Due to the strong winds (about 15 m/s) during the monsoon, air-sea gas exchange had restored the CFC-12 saturations to near the equilibrium with the atmosphere in August–September (Fig. 3c).

Intermediate waters

In April 1995, a surprising feature was found in the Gulf of Oman. At about 300 m depth, which corresponds to the salinity maximum and the density of the Persian Gulf Water (PGW), elevated CFC-12 concentrations were observed. The CFC-12 values were highest at the north-western stations near the shelf (Fig. 4a, page 18), similar to the other extrema like salinity and oxygen. There, CFC-12 saturations of PGW exceeded 250% (Rhein et al., 1997). These supersaturations were also found in August 1995 (Rana Fine, pers. comm.) but are usually not observed in the ocean. In the Persian Gulf, this water mass was probably contaminated with oil, and the lipophilic character of the CFCs led to the observed supersaturations. At the eastern exit of the Gulf, the intermediate CFC-12 maximum is still visible, but the CFC-12 concentrations at the depth of the PGW decrease farther away from the Gulf (Fig. 4b, page 18).

South of 2°N at km 3000, however, the depth and density range of the PGW exhibits higher CFC values than observed between 12°N and 20°N (Fig. 4b). The enhanced CFC signals south of the equator characterizes Indian Central Water (ICW), which is formed south of 40°S (You and Tomczak, 1993). It seems that the CFC load of the ICW flowing into the Arabian Sea plays an important role for the CFC budget of the Arabian Sea in this density range (Rhein et al., 1997). This is not the case for the depth layers between 500 m and 1000 m depth, where the CFC-12 signals south of the equator are lower than the values found in the Arabian Sea (Rhein et al., 1997).

The third source delivering CFCs mainly to intermediate layers of the Arabian Sea at depths between 500 and 1000 m is the outflow from the Red Sea (Red Sea Water, RSW). The CFC maximum is clearly visible in the Gulf of Aden (Fig. 4c, page 18), CFC-12 saturations at the Strait of Bab el Mandeb were 65% at 400 m depth. The

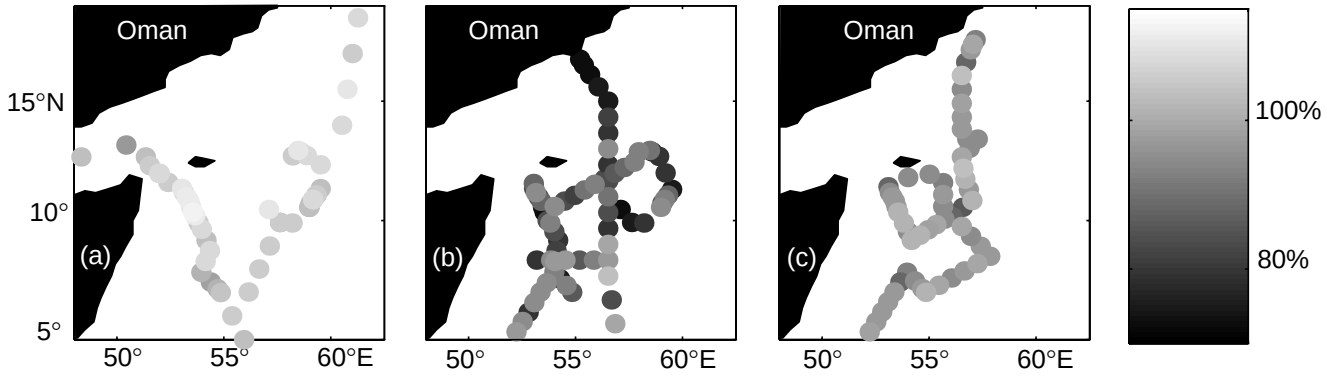

Figure 3. CFC-12 surface saturation (a) in March–April 1995 (cruise M32/1), (b) in June–July 1995 (cruise M32/4), and (c) in August–September 1995 (cruise M32/6).

saturation decreased to 50% while descending to depths around 800 m just east of the Strait. There, the CFC and oxygen saturation of RSW (800 m depth: CFC-12: 50%, O_2: 23%) are significantly lower than for PGW at the exit of the Gulf of Oman (CFC-12: 100%, O_2: 33%), reflecting the fact that the RSW contains deep and intermediate water masses from the Red Sea, which were sealed off the surface for some time.

The inflow of ICW into the intermediate layer of the Arabian Sea was estimated with a two-box model for the region north of 12°N. ICW inflows between 0.2 and 0.9 Sv (Box 1, $\sigma_\theta = 26.5 - 27.0$, about 300 m–500 m depth) and between 1 and 6 Sv (Box 2, $\sigma_\theta = 27.0 - 27.4$, about 500 m–1000 m depth) were able to satisfy the CFC budget of the Arabian Sea (Rhein et al., 1997). The strength of the modelled total ICW inflow was mainly dependent on the flow of RSW into the region north of 12°N. Most likely, only a fraction of the 0.4 Sv RSW (Siedler, 1968) which enters the Gulf of Aden flows northward, the salinity maximum of RSW was observed as far south as the Agulhas Current (Gordon et al., 1987).

Oxygen consumption rates

Knowing the strength of the inflowing water masses and their oxygen concentrations, the oxygen consumption rate of the intermediate depths of the Arabian Sea north of 12°N can be estimated. This region is characterized by the thickest low-oxygen layer today (Olson et al., 1993). In March-April 1995, the oxygen concentrations of PGW and RSW were found to be 1.6 ml/l and 1.3 ml/l, respectively. The mean oxygen concentrations for ICW south of the equator were 2.0 ml/l ($\sigma_\theta = 26.5 - 27.0$) and 1.2 ml/l ($\sigma_\theta = 27.0 - 27.4$). We assume that 0.18 Sv PGW (Koske, 1972) enter Box 1, and 0.3 Sv RSW enter Box 2. The strength of the ICW inflow is taken from the model of Rhein et al., 1997 (0.55 Sv, Box 1 and 3.0 Sv, Box 2). The mean oxygen concentrations in the intermediate layers of the Arabian Sea north of 12°N were found to be 0.21 ml/l for the density range $\sigma_\theta = 26.5 - 27.0$ (Box 1) and 0.16 ml/l for $\sigma_\theta = 27.0 - 27.4$ (Box 2). The calculated oxygen consumption rates of 0.06 ml/lyear (Box 1, about 300–500 m depth) and 0.16 ml/lyear (Box 2, about 500–1000 m depth) are in the same order of magnitude than the estimates of Olson et al. (1993).

Acknowledgements

We thank captain and crew of RV Meteor for their support during the field measurements. T. Elbrächter performed many of the CFC analyses. Funding was provided by the Bundeministerium für Bildung, Wissenschaft, Forschung und Technologie (BMBF), WOCE grant 03F0157A. The Meteor cruises were supported by the Deutsche Forschungsgemeinschaft (DFG).

References

Gordon, A. L., J. R. E. Lutjeharms, and M. L. Gründlingh, 1987: Stratification and circulation at the Agulhas Retroflection. Deep-Sea Res., 34, 565–599.

Haine, M. A., M. E. Luther, and R. A. Fine, 1997: Mixed layer gas saturations in the northwestern Indian Ocean, model and observations. Geophys. Res. Lett., submitted.

Koske, P. H., 1972: Hydrographische Verhältnisse im Persischen Golf aufgrund von Beobachtungen von FS Meteor im Frühjahr 1965. Meteor Forschungsergebnisse, A11, 58–73.

Olson, D., G. L. Hitchcock, R. Fine, and B. A. Warren, 1993: Maintenance of the low oxygen layer in the central Arabian Sea. Deep-Sea Res., 40, 673-685.

Rhein, M., L. Stramma, and O. Plähn, 1997: Tracer signals of the intermediate layer of the Arabian Sea. Geophys. Res. Lett., in press.

Schott, F., J. Fischer, U. Garternicht, and D. Quadfasel, 1997: Summer monsoon response of the northern Somali Current, 1995. Geophys. Res. Lett., in press.

Siedler, G., 1968: Schichtungs- und Bewegungsverhältnisse am Südausgang des Roten Meeres. Meteor Forschungsergebnisse, A4, 1–76.

Warner, M. J., and R. F. Weiss, 1985: Solubilities of chlorofluorocarbons 11 and 12 in water and seawater. Deep-Sea Res. 32, 1485–1497.

You, Y., and M. Tomczak, 1993: Thermocline circulation and ventilation in the Indian Ocean derived from water mass analysis. Deep-Sea Res., 40, 13–56.

1998 International Year of the Ocean

In recognition of the importance of the ocean, the marine environment and its resources for life on earth and for sustainable development, the United Nations has declared 1998 as the International Year of the Ocean. This provides a window of opportunity for governments, organisations and individuals to become aware of the ocean situation and to consider the actions needed to undertake our common responsibility to sustain the greatest common heritage we have and without which we cannot exist.

In connection with this the IOC launched its 1998 IYO webserver:

http://www.unesco.org/ioc/iyo/iyohome.htm

The objective of this server is to provide up-to-date information on 1998 IYO activities around the world. Visit this page regularly to find more about:

- history on how the idea for the IYO came about
- what the IYO is all about
- how the organisation and co-ordination is arranged for the IYO and how it all works
- update calendar of all activities which are being planned: Ocean Charter, Ocean Education, Public Information, Ocean Awards, Conferences, Research and Training Cruises, Publication, Stamps etc.
- EXPO'98: The Oceans, a heritage for the future, Lisbon 22 May–30 September 1998.

Send information on activities planned for the IYO or ask for more information through: Iouri Oliounine or Florence Taylor, UNESCO-IOC, 1 rue Miollis, 75732 Paris Cedex 15, France, Tel: (33 1) 45683963, Fax: (33 1) 45685812, e-mail i.oliounine/f.taylor@unesco.org.

Updated Transatlantic Heat Flux at 26.5°N

W. E. Johns, T. N. Lee, R. J. Zantopp, and E. Fillenbaum, RSMAS, University of Miami, USA. zantopp@rsmas.miami.edu

Determining the patterns and amounts of heat transported in the world ocean is of great importance to our understanding of ocean circulation and its influence on climate. At the present time, most available estimates of meridional ocean heat flux are based on single hydrographic sections, which are often assumed to be representative of the mean state of the ocean. To improve estimates of ocean heat flux, it was concluded in early WOCE planning that hydrographic data collected over a full zonal section would need to be combined with time series measurements of current and temperature in the energetic western boundary layer at approximately the same latitude.

Here we highlight results from an implementation of this strategy along 26.5°N in the Atlantic, where long-term time series of current and temperature from the WOCE ACM-1 moored array east of the Bahamas (Fig. 1) have been combined with Florida Current transports and interior hydrographic data to update the estimate of transatlantic heat flux (Lee et al., 1996; Fillenbaum et al., 1997). Estimates of the annual mean and seasonally varying meridional heat flux at this latitude are given and compared with results from the first generation CME (Community Modeling Effort) model of the North Atlantic (hereafter CME-1; Bryan and Holland, 1989).

The mean meridional velocity structure for three deployments of ACM-1 between 1987 to 1992 is shown in Fig. 1. The mean flow structure is remarkably consistent between the deployment periods, showing: (i) a mean

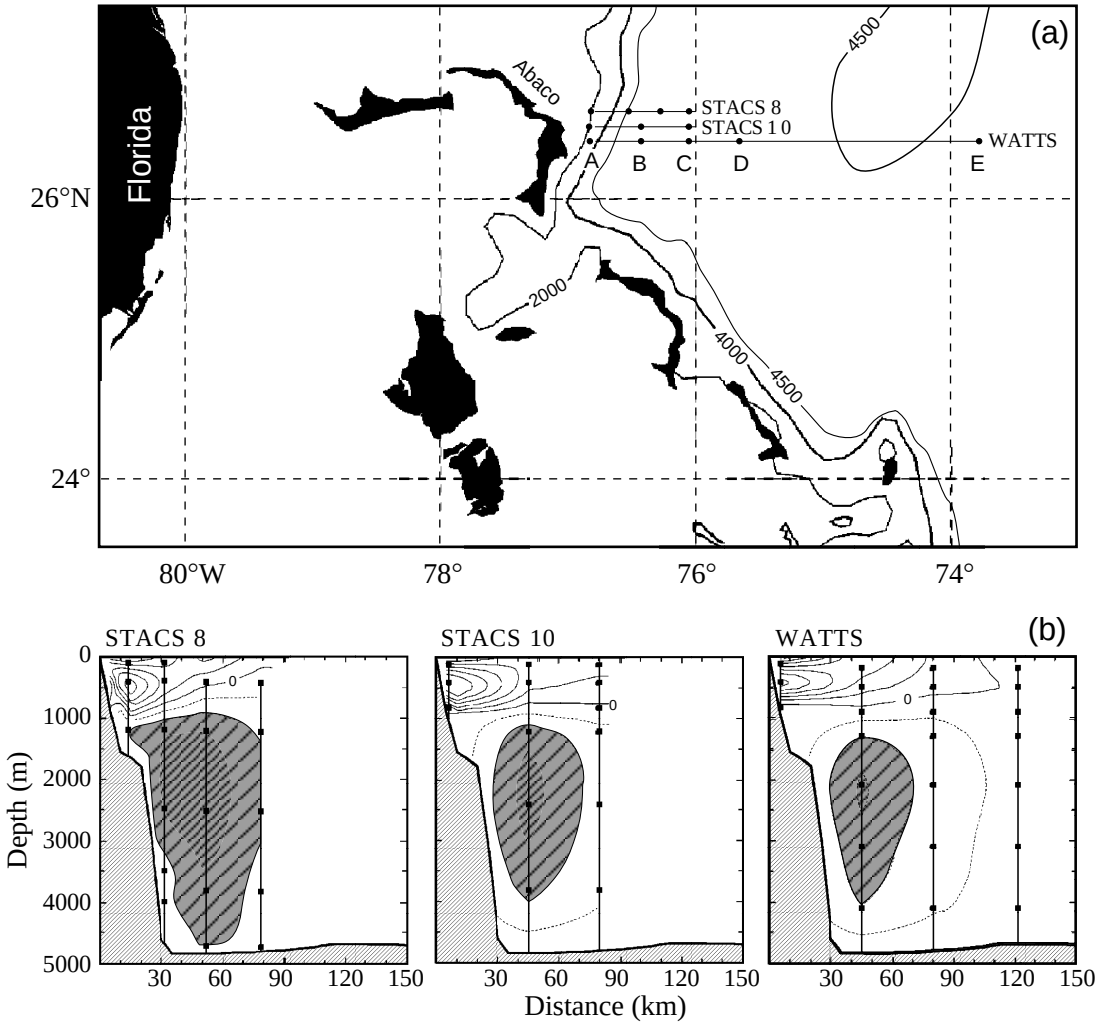

Figure 1. (a) ACM-1 arrays off Abaco, Bahamas, from 1987–1992 (individual arrays in chronological order are labelled STACS-8, STACS-10, and WATTS). All moorings were deployed along 26.5°N, and are shown offset here for clarity. (b) Mean meridional velocity structure for each array period. Contour interval is 5 cm/s; southward flow in the DWBC greater than 10 cm/s is hatched.

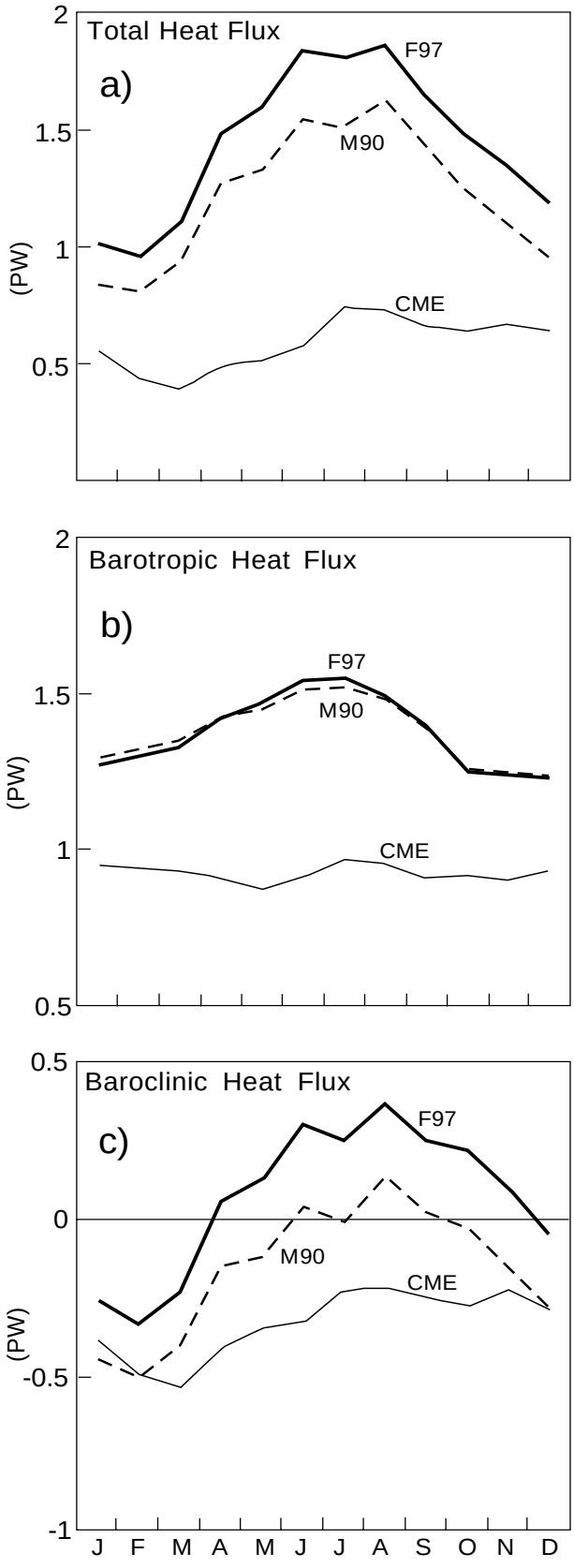

Figure 2. Monthly averages of transatlantic heat flux from Fillenbaum et al., 1997 (F97), compared with the results of Molinari et al., 1990 (M90) and the CME-1 (CME); (a) total heat flux, (b) barotropic heat flux, and (c) baroclinic heat flux.

Antilles Current as a northward jet against the Bahamas escarpment centred near 400 m depth with a core velocity of 30 cm/s, and (ii) a well-organized Deep Western Boundary Current (DWBC) below 800 m with a core of 10–15 cm/s near 2500 m. The observed northward flow above 800 m has a mean transport of 5±1.8 Sv, and the deep southward flow has a mean of -27±3.7 Sv. The CME-1 exhibits a similar flow structure off Abaco but has a stronger northward mean transport above 800 m of approximately 10 Sv and a weaker southward DWBC of -17 Sv.

Following Bryden and Hall (1980), the transatlantic heat flux calculation is broken down into regional "barotropic" and "baroclinic" heat transport contributions:

$$Q = \rho C_p \left\{ \int_0^L H\bar{v}\bar{\theta}dx + \int_0^L \int_0^{H(x)} v'\theta' dz dx \right\}$$

where an overbar denotes a depth average and a prime denotes a deviation from that average. H is the ocean depth, and the other notation is standard. In previous applications at 24–27°N in the Atlantic (Hall and Bryden, 1982; Molinari et al., 1990), the barotropic heat transport is calculated using direct measurements in the Florida Current and assuming that the measured northward flow through the Straits of Florida is balanced by an equivalent southward flow through the ocean interior at a basin-averaged mean temperature. Corrections to this scheme are necessary where significant transports occur over regions of relatively shallow topography in the interior (e.g., at the western and eastern boundaries or over interior topographic features such as mid-ocean ridges; Hall and Bryden, 1982). The baroclinic heat transport contains a geostrophic part, calculated from temperature and geostrophic velocity profiles across the interior (and either geostrophic or direct measurements in the Florida Current), and an Ekman contribution calculated by assuming that the surface Ekman transport at a mean mixed layer temperature is balanced by a deeper return flow at the interior mean temperature.

Application of this method by Molinari et al. (1990) to monthly mean Florida Current data and monthly Levitus (1982) averages in the interior led to an estimate of 1.21 ±0.34 PW for the annual mean meridional heat flux across 26.5°N, with a seasonal range of over 1 PW, from 0.7 PW in February to 1.9 PW in July. Differences in the methodology when incorporating the ACM-1 data are (Fillenbaum et al., 1997): (i) the mean annual cycles of barotropic heat and volume transports from ACM-1 are combined with the respective estimates for the Florida Current, and the (smaller) mass flux residuals are then balanced with monthly interior mass fluxes, and (ii) direct baroclinic heat transports calculated from the ACM-1 array are used to replace Levitus estimates in the western boundary layer.

The results of this calculation yield a revised estimate of 1.44±0.33 PW for the total transatlantic heat flux, with an annual range of 0.8 PW and maximum heat flux occurring in summer (Fig. 2a). The 0.2 PW increase in the annual mean heat flux over the 1.2 PW value estimated by Molinari

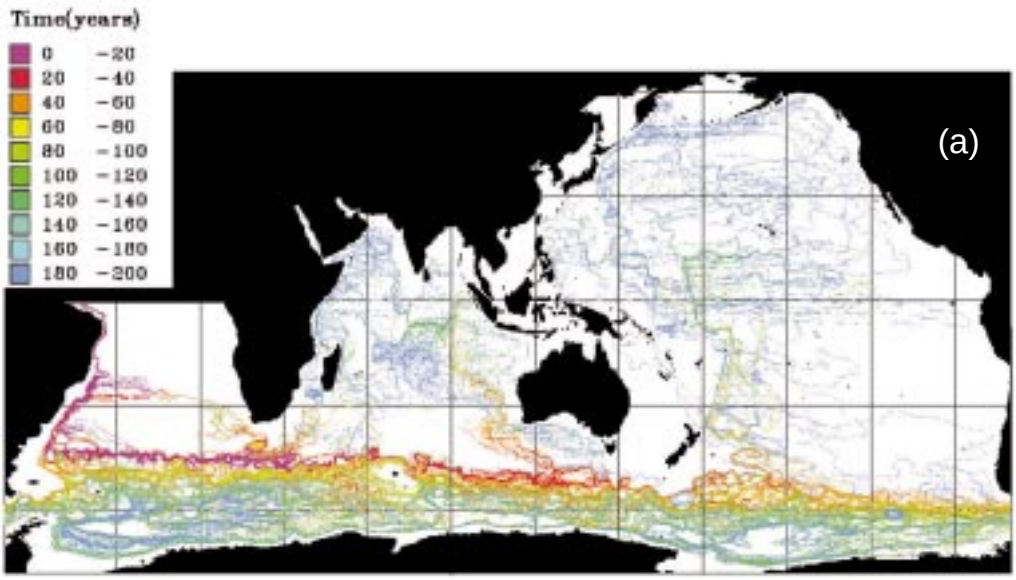

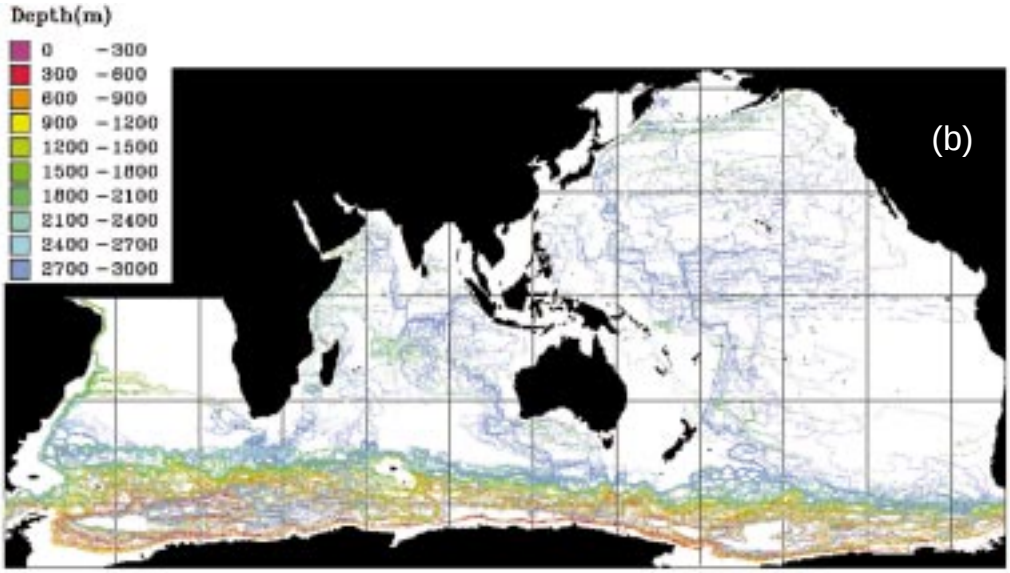

Döös and Coward, page 3, *Figure 1. A selection of 200 NADW trajectories, released at the equator in the Atlantic and followed until the water is transformed into water lighter than* $\rho_0 = 1027.625\ kg/m^3$. *As a function of (a) time and (b) depth.*

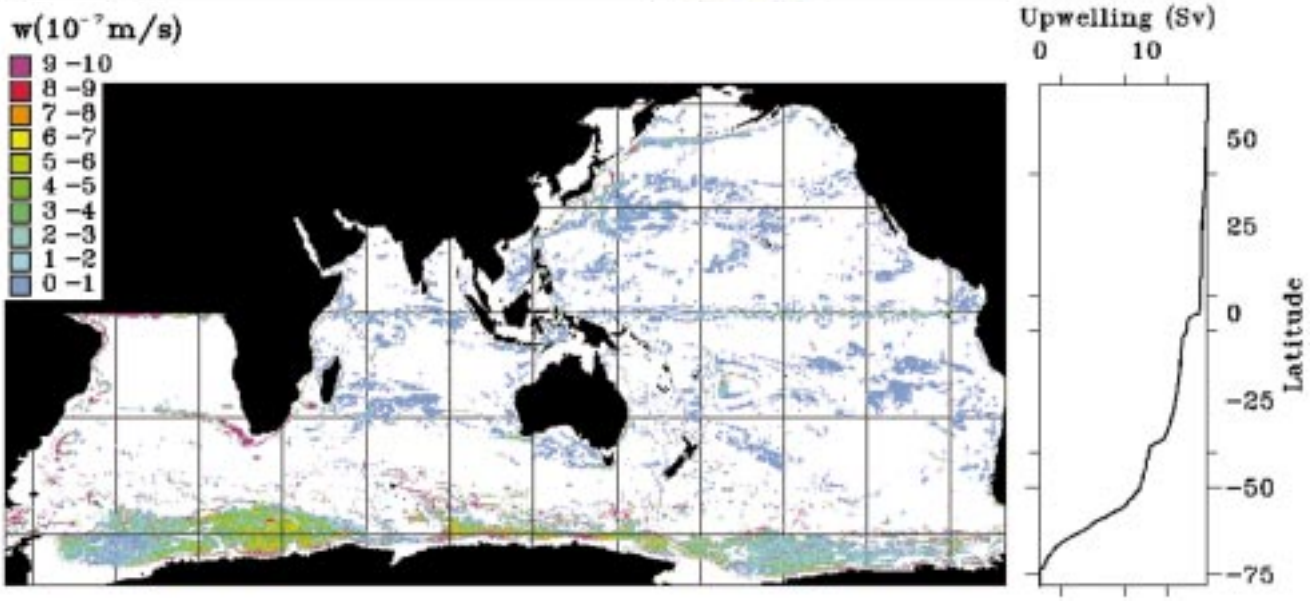

Döös and Coward, page 4, *Figure 2. Vertical velocity of the originally North Atlantic Deep Water as it reaches the isopycnal* $\rho_0 = 1027.625\ kg/m^3$ *calculated from 1.58 million trajectories and the corresponding meridionally integrated transport from Antarctica and northward. The total transport of NADW is* $15.8 \times 10^6\ m^3/s$.

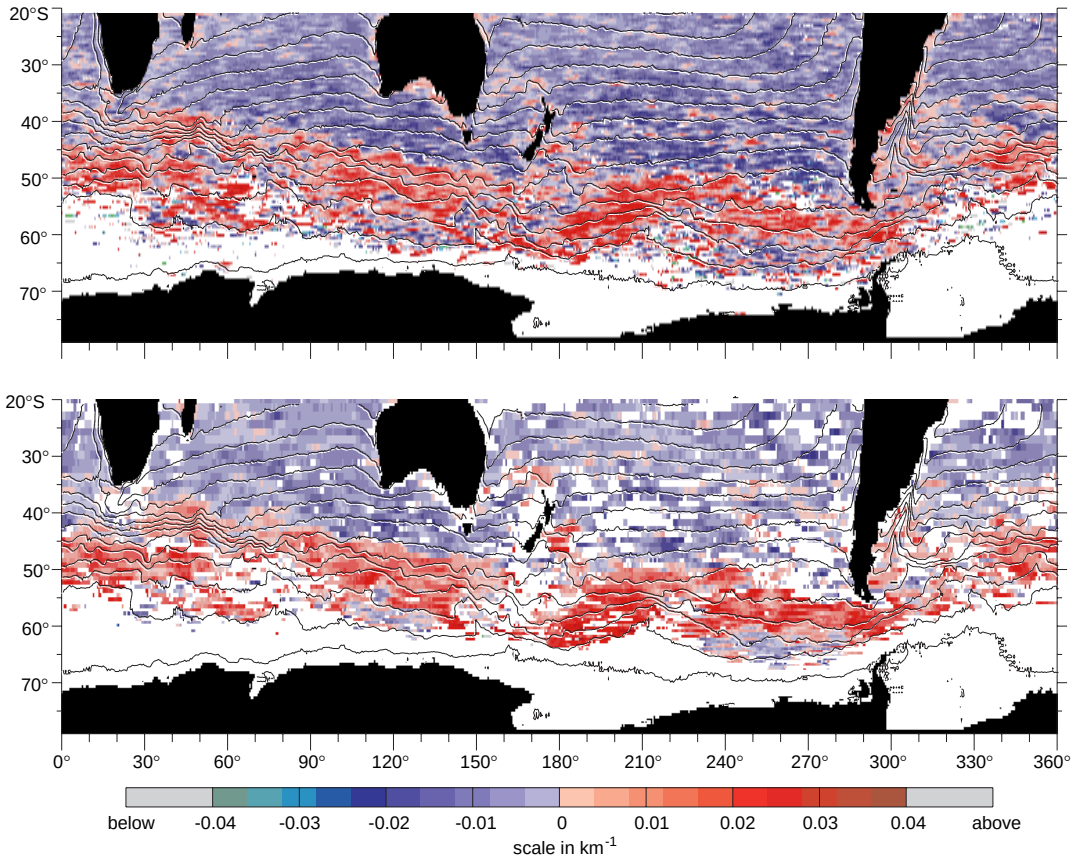

Hughes, page 6, *Figure 1. Zonal wavenumbers calculated from (top) ATSR and (bottom) ERS-1 altimeter data. Positive (red) values represent eastward propagation. Contours are mean sea surface temperature, from ATSR, at intervals of 2°C.*

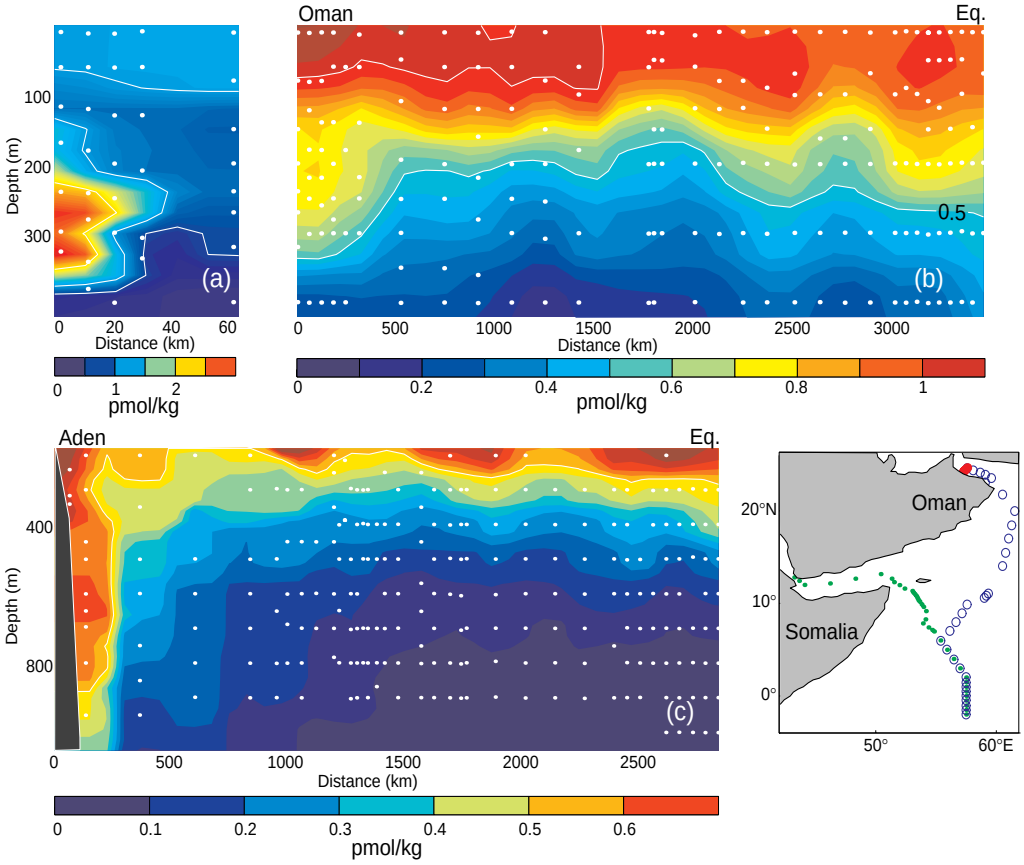

Rhein et al., page 13, *Figure 4. Vertical distribution versus distance for CFC-12, March–April 1995. The location of the sections are shown in the inset map. (a) CFC-12 distribution in the upper 400 m along the northernmost section in the Gulf of Oman, beginning at the shelf at km 0 (location of the section: red dots in inset map). (b) CFC-12 distribution in the upper 400 m from the Gulf of Oman to 2°S (location of the section: blue circles in map). (c) CFC-12 section for the 200 m–1000 m depth range from the Gulf of Aden to 2°S (location of the section: green dots in map). Note the different CFC-12 colourscale for Figures 4a, b, and c.*

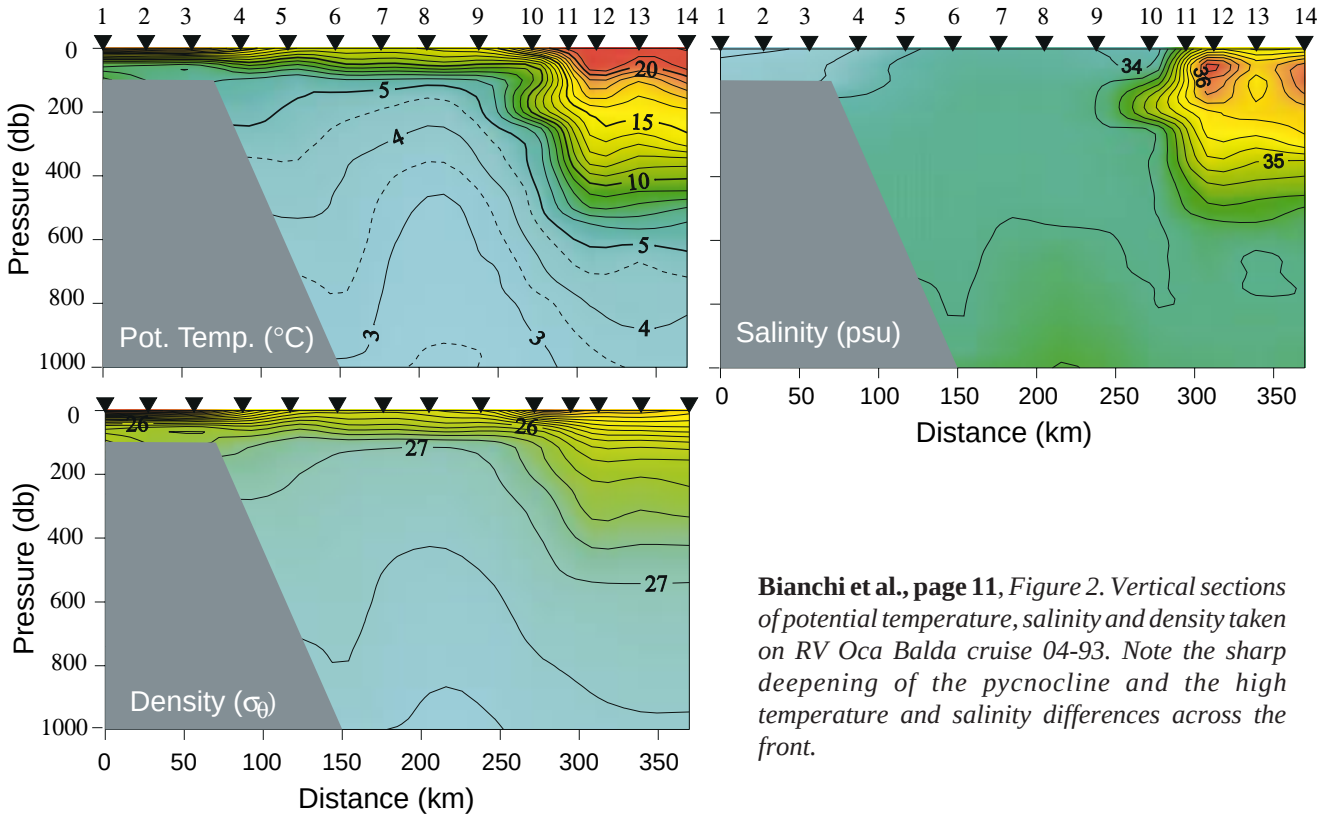

Bianchi et al., page 11, *Figure 2. Vertical sections of potential temperature, salinity and density taken on RV Oca Balda cruise 04-93. Note the sharp deepening of the pycnocline and the high temperature and salinity differences across the front.*

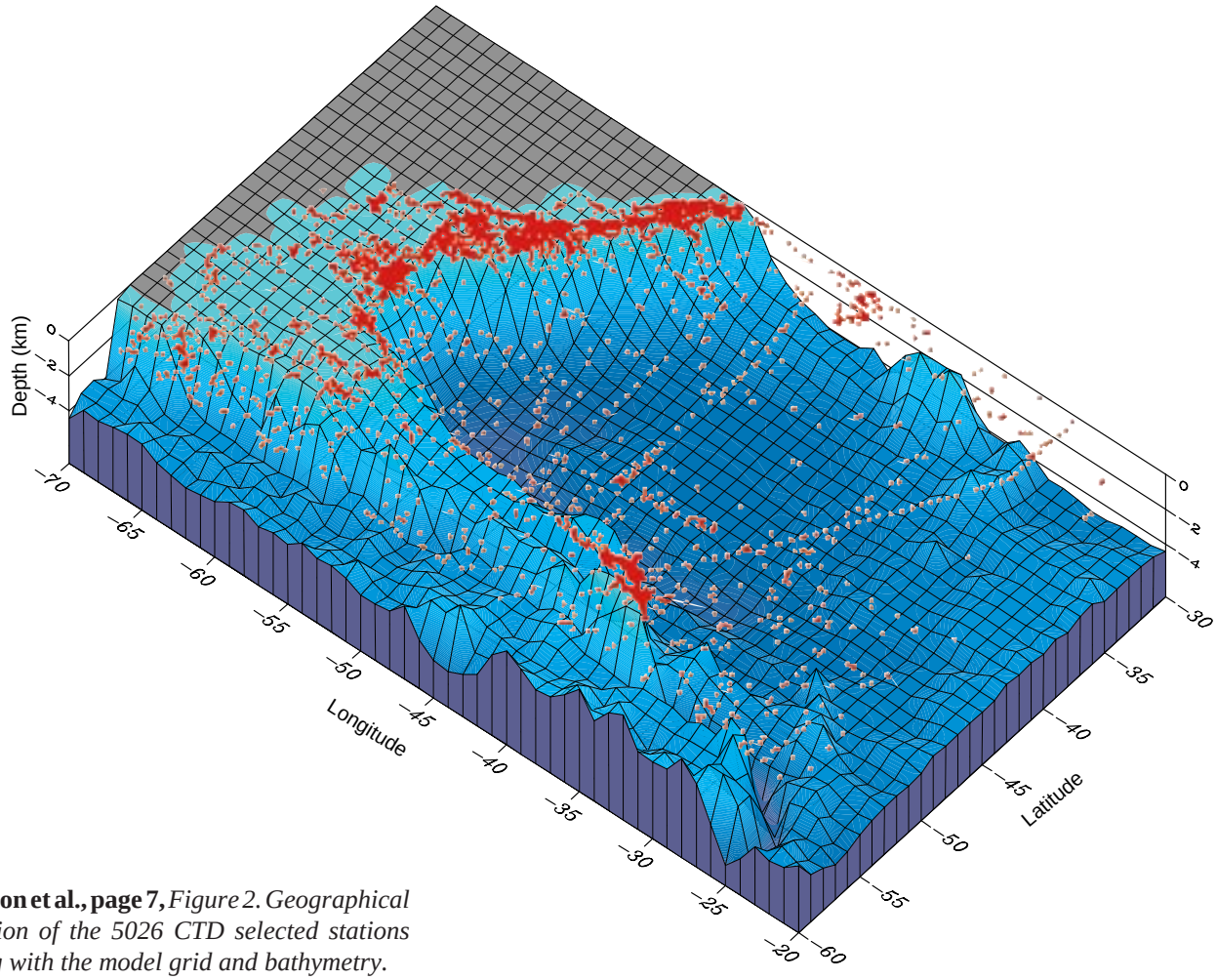

Garçon et al., page 7, *Figure 2. Geographical location of the 5026 CTD selected stations along with the model grid and bathymetry.*

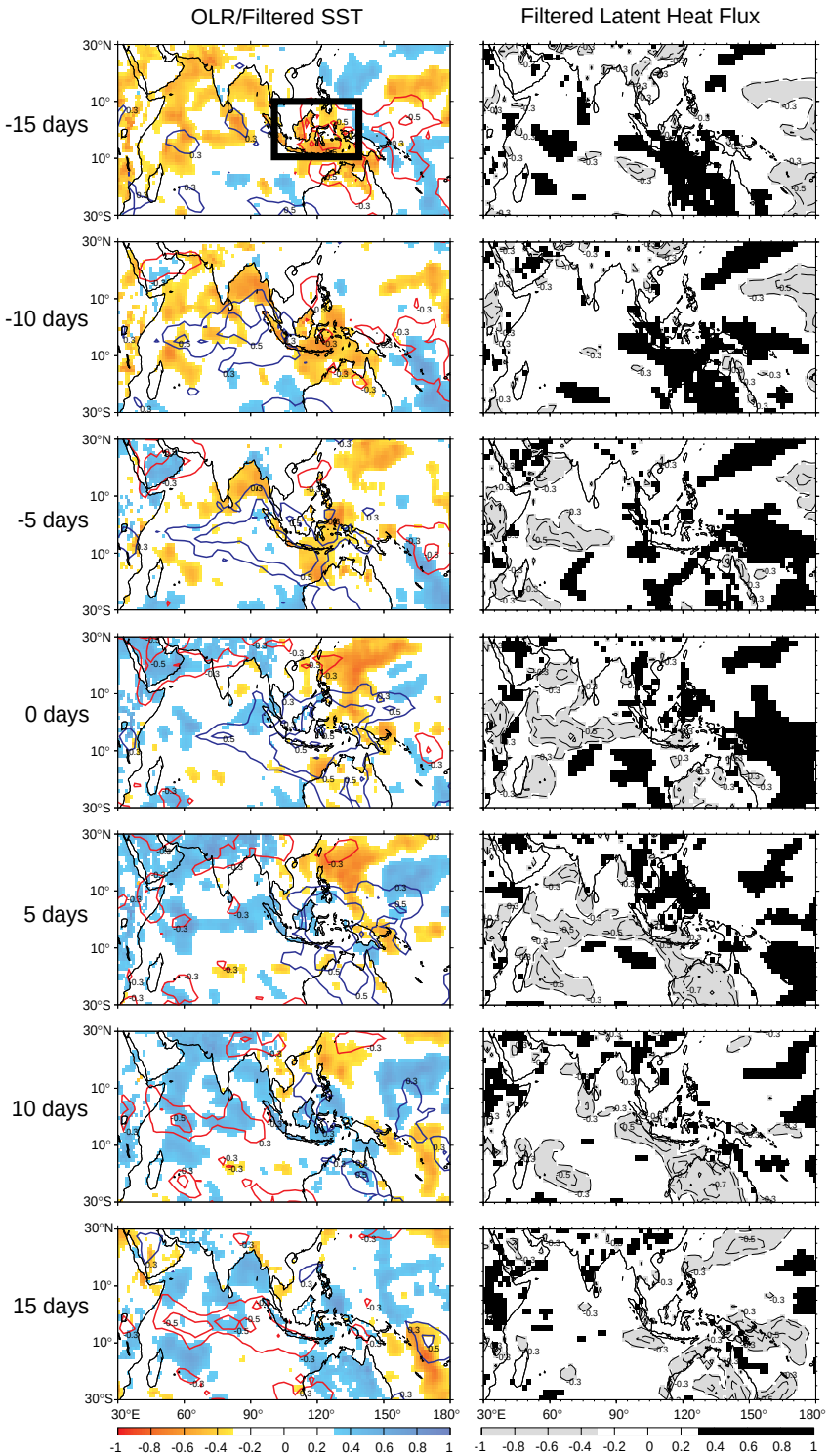

Sperber and Slingo, page 30, *Figure 1. Lagged correlations of the pentad averaged IO index with total OLR and 20–100 day bandpass filtered SST (and surface skin temperature over land from the ECMWF reanalysis) are plotted in the left-hand column. Correlations with the OLR are plotted as contours with positive correlations (blue isolines) indicating enhanced convection and negative correlations (red isolines) indicating suppressed convection during the active phase of the IO. The correlations with the filtered SST are plotted as gridpoint data where negative correlations (shaded yellow-red) correspond to warm SST anomalies and positive correlations (shaded light blue-dark blue) correspond to cold SST anomalies during the active phase of the IO. In the right-hand column the lagged correlations of the pentad averaged IO index with 20–100 day bandpass filtered latent heat flux are plotted. Negative correlations (shaded light grey) correspond to enhanced evaporation and positive correlations (shaded black) correspond to below normal evaporation during the active phase of the IO. Correlations significant at ≥95% confidence level (|r| ≥0.3) are plotted. The box in the upper left-hand panel is the region from which the IO index was obtained.*

et al. (1990) is due almost entirely to a larger baroclinic heat flux in the ACM-1 region obtained from direct measurements, compared to that derived from the Levitus climatology, which does not adequately resolve the strong shear between the Antilles Current and the DWBC along the western boundary.

The annual cycle of transatlantic heat flux calculated directly from the CME-1 is also shown in Fig. 2, along with its breakdown into barotropic and baroclinic components. It can be seen that in addition to having too weak an annual mean heat flux, the model has a much weaker annual cycle than indicated by observations. The reasons for the lower mean value are known (Bryan and Holland, 1989) and can be attributed primarily to an inadeqacy in the "sponge layer" boundary conditions that drive the large scale overturning cell in this version of the model. This has been improved in more recent simulations (e.g., Doscher et al., 1994). However, it is not obvious why the annual cycle in the CME-1 should be so small compared to observations, which in a sense may be considered an even more fundamental disagreement. The model exhibits a weak annual cycle for the baroclinic heat flux that is roughly in phase with observations but almost no variation in the barotropic heat flux. To clarify the reasons for these differences, it is useful to break down the model heat transport into component terms using the same methodology that is applied to the observations (Fig. 3).

Variations in the barotropic heat flux in both model and observation are related primarily to changes in the volume transport and mean temperature of the Florida Current. As shown in Fig. 3a, the observed annual cycle of the Florida Current varies over a range of 6 Sv, whereas the CME-1 cycle has only about one-third this amplitude and somehat different phase. Both cycles show a fall minimum, but the summer maximum in the observed transport is only weakly evident in the model. Furthermore, the annual cycle of the mean Florida Current temperature in the model is nearly out of phase with the transport, such that the effect of the fall transport minimum is largely supressed by the fall maximum in temperature. A similar cycle is seen in the observed temperature, but it has a much smaller net effect due to the dominance of the volume transport cycle.

Annual cycles of the various components of the baroclinic heat flux are shown in Fig. 3b–d. The annual cycles of the Ekman and Florida Current contributions are very similar between the observations and model, even though the Florida Current contribution from the model is about 0.1 PW higher in the mean. The major discrepancy between the model and observations is in the contribution due to interior geostrophic flow, where the annual cycles

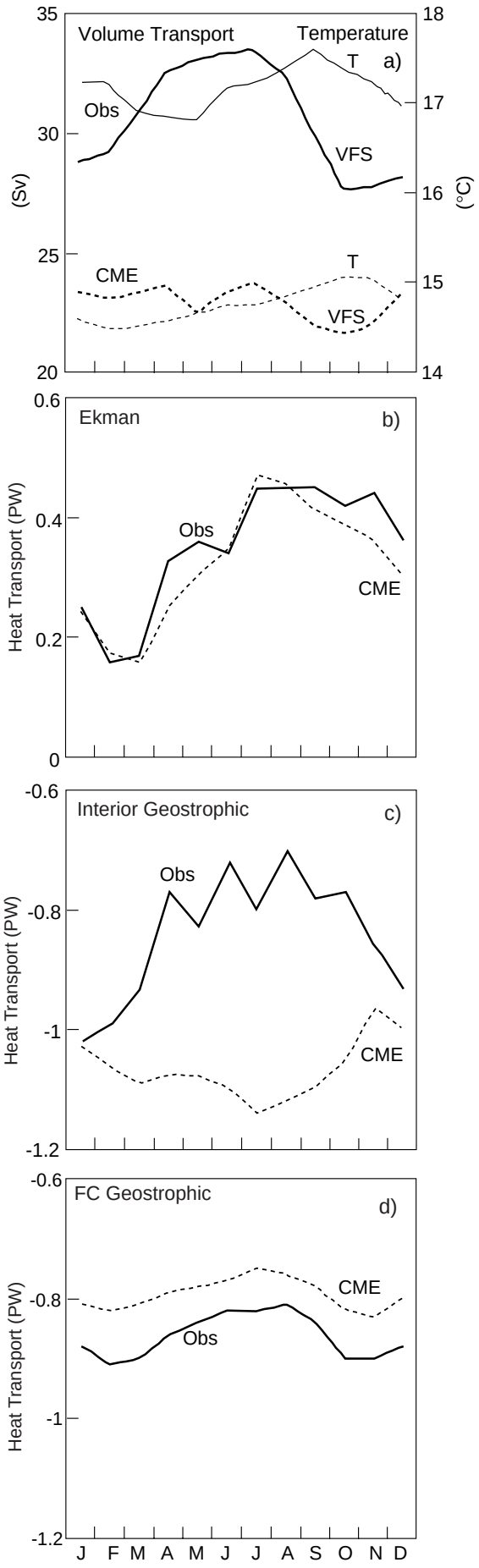

Figure 3. Individual terms in the transatlantic heat flux calculation, from observations (Fillenbaum et al., 1997) and the CME-1: (a) Florida Straits monthly average volume transport (VFS) and potential temperature (T); (b) Ekman heat transport; (c) interior baroclinic heat transport due to geostrophic flow; and (d) Florida Straits baroclinic heat transport.

are essentially out of phase. The model annual cycle has a weak (southward) minimum in summer, whereas the observed annual cycle, calculated from Levitus climatology and ACM-1 data, has a broad maximum in summer with nearly three times the amplitude (annual range of ~0.3 PW). Most of this signal is contributed by the Levitus interior cycle. As discussed by Böning and Herrmann (1994), the CME's annual heat flux cycle in subtropical latitudes is almost completely due to the Ekman contribution, consistent with theoretical expectations that there is little baroclinic adjustment of the gyre circulation on the annual time scale. In view of this, the relatively large amplitude of the observed baroclinic heat flux cycle is puzzling. It is not immediately clear that the CME has to be incorrect; indeed, it is possible that due to irregular sampling and eddy contamination, the Levitus (1982) climatology may not be representative of the true interior annual cycle. Further study is needed to resolve this discrepancy. Improvement of the Levitus interior estimate may be possible using the AX7 repeat VOS XBT line across the Atlantic, which was upgraded to quarterly high-resolution sampling in 1994 (Molinari and Baringer, NOAA/AOML).

In summary, we find that the small annual cycle of meridional heat flux in the CME 1 compared to observations is due primarily to the weak annual cycle of the Florida Current in the model, and the lack of a significant geostrophic heat flux variation across the interior.

An effort is now underway to establish interannual monitoring of transatlantic heat flux at 26.5°N using ongoing Florida Current measurements, ACM-1 measurements east of the Bahamas, and VOS XBT measurements across the interior. Further comparisons of the observed heat flux cycle and its regional components with modeling efforts would be very useful in determining possible inadequacies in either models or observations, as well as important differences between models. Properly simulating the climatological mean and annual cycle of the meridional heat flux will be an important starting point for simulation of interannual or decadal ocean heat transport variability.

References

Böning, C. W., and P. Herrmann, 1994: On the annual cycle of poleward heat transport in the ocean: Results from high resolution modeling of the North and Equatorial Atlantic. J. Phys. Oceanogr, 24, 91–107.

Bryan, F., and W. Holland, 1989: A high resolution simulation of the wind and thermohaline-driven circulation in the North Atlantic Ocean. Parametrization of Small-Scale Processes, Proc. Aha Huliko'a Hawaiian Winter Workshop. P. Müller and D. Anderson, Eds., University of Hawaii at Manoa, 99–115.

Bryden, H. L., and M. M. Hall, 1980: Heat transport by currents across 25°N latitude in the Atlantic Ocean. Science, 207, 884–886.

Döscher, R., C. W. Böning, and P. Hermann, 1994: Response of the circulation and heat transport in the North Atlantic to changes in thermohaline forcing in northern latitudes: A model study. J. Phys. Oceanogr., 24, 2306–2320.

Fillenbaum, E. R, T. N. Lee, W. E. Johns, and R. J. Zantopp, 1997: Meridional heat transport variability at 26.5°N in the North Atlantic. J. Phys. Oceanogr., 27, 153–174.

Hall, M. M., and H. L. Bryden, 1982: Direct estimate and mechanism of ocean heat transport. Deep-Sea Res., 29, 3A, 339–359.

Lee, T. N., W. Johns, R. Zantopp, and E. Fillenbaum, 1996: Moored observations of western boundary current variability and thermohaline circulation at 26.5°N in the subtropical North Atlantic. J. Phys. Oceanogr., 26, 962–983.

Levitus, S., 1982: Climatological Atlas of the World Ocean. NOAA Prof. paper 13, US Govt. Print. Office. 173 pp.

Molinari, R. L., E. Johns, and J. F. Festa, 1990: The annual cycle of meridional heat flux in the Atlantic Ocean at 26.5°N. J. Phys. Oceanogr., 20, 476–482.

Global Ocean Data Assimilation Experiment (GODAE)

On-going ocean applications are encouraging interest in a range of global ocean modelling and observing activities. In order to address these needs the Ocean Observing Panel for Climate is proposing a Global Ocean Data Assimilation Experiment (GODAE). GODAE aims to show the practicality and viability of routine, real-time global ocean data assimilation and prediction. GODAE will demand significant integration, observing and modelling components, such as is being promoted in research programmes like WOCE. The objectives of GODAE include: open-ocean information to improve the predictability of coastal ocean systems; a method for routine handling, quality control and interpretation (analysis) of ocean data sets; a description of the ocean circulation and physics upon which specialised systems, such as biological models, can be developed and tested; initial conditions for climate predictions, and analyses for validation of climate simulations; and a unifying target for various research enterprises (observational, theoretical and modelling).

The experiment depends upon a variety of space-borne systems, a global in-situ ocean observation network, and global circulation models. The realisation of GODAE depends on significant scientific challenges. Present determinations of surface forcing must be improved. Appropriate suite of direct measurements will emerge from global and regional studies of ocean variability. There must be improvements in high-resolution global ocean models capable of simulating the true global circulation and assimilating many types of data. And there must be significant enhancements in communications and telemetry. The synthesis phase of WOCE is critical for meeting these challenges. Without substantial progress in WOCE, real-time global ocean modelling and data assimilation may not be feasible. The timing and duration of the experiment (tentatively 2003–2005) depend on plans of space agencies and on our ability to realise an appropriate direct observation network.

The definition of the experiment is currently being debated. GODAE needs a productive and co-operative working relationship with WOCE, CLIVAR, and the many individuals and groups who have a scientific interests in these areas. Further information is available at http://WWW.BoM.GOV.AU/bmrc/mrlr/nrs/oopc/godae.htm.

Improved Representation of Flow Around Topography in the GFDL Modular Ocean Model MOM 2

Anand Gnanadesikan and Ronald C. Pacanowski, AOS Program, Princeton University and NOAA/GFDL. rcp@gfdl.gov

The GFDL Modular Ocean Model MOM 2 (Pacanowski 1996) and its descendants (Pacanowski et al., 1991; Cox, 1984; Semtner, 1974; Bryan, 1969) have traditionally used a vertical discretization which forces all grid points within the same level to lie at the same depth. As noted by Gerdes (1993), this discretization results in a number of problems. In particular:

1. A poorly resolved bottom. In regions of weak slopes (where grid aspect ratio $\Delta z/\Delta x$ > slope), high vertical resolution is needed to resolve the slope. When poorly resolved, the effect is to replace a gentle slope with sharp jumps in topography.
2. Absence of dynamical overflows. In density driven overflow regions, friction plays an important role, and the slope of the top of the plume follows that of the bottom. Pure level coordinate models cannot produce a frictional plume unless they have very large vertical resolution (so that the Ekman depth is roughly the same as the grid spacing). Furthermore, the pressure gradient driving such a plume will be incorrect unless horizontal resolution is also very high.

At present, solving both of these problems within a z-coordinate ocean model is not feasible, since problem 1 requires very high vertical resolution (or very low horizontal resolution) in regions of weak slopes, and problem 2 requires very high horizontal resolution in regions of strong slopes. Recent work at GFDL has suggested that by making a minor adjustment to a pure level-coordinate, one can obtain significant improvements for relatively low computational costs.

Instead of using cells which all have the same height, the bottom-most ocean cell is allowed to be a "partial" cell in the sense that it is partially filled by land (similar to the "shaved" cells suggested by Adcroft et al., 1997). Such an approach allows for topography to vary continuously. However, unless care is taken in the formulation of the diffusion and pressure gradient terms, problems found in sigma coordinate models can result. In particular, an initial

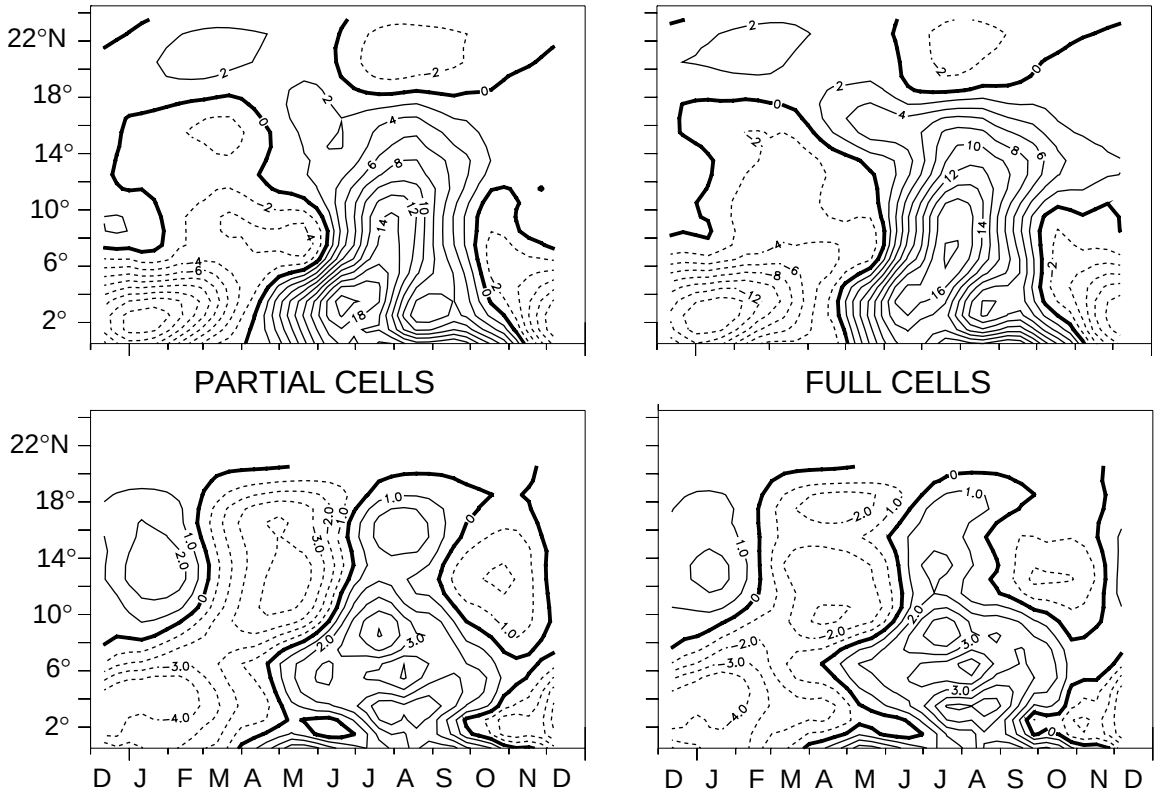

Figure 1. Annual cycle of gyre strengths in the Indian Ocean. All plots are of zonally averaged streamfunction from the fifth year of integration, giving some measure of the strength of particular gyres. Upper: Zonally averaged streamfunction in the western basin (38°E–75°E) using partial cells (left) and full cells (right). Lower: Zonally averaged streamfunction in the eastern basin (80°E–100°E) using partial cells (left) and full cells (right).

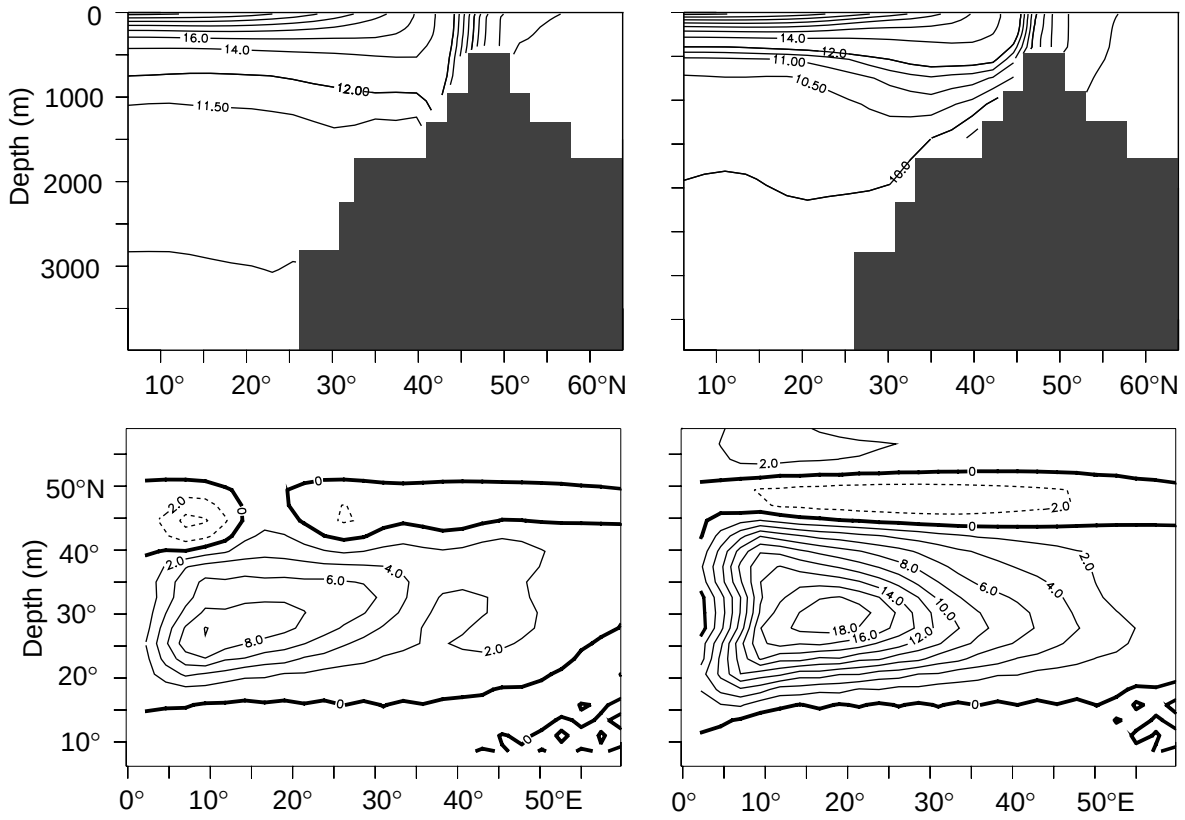

Figure 2. Illustration of the difference produced in an idealized basin by the addition of a bottom boundary layer. Upper: Zonally averaged temperature (0°E–60°E) for the case without a bottom layer (left) and with a bottom boundary layer (right). Note the position of the 11°C isotherm at around 3000 m in the left panel and at 500 m with a different shape of the thermocline in the right panel. Lower: Streamfunction after 160 years without a bottom boundary layer (left), with a bottom boundary layer (right). Note the strengthening of the subtropical gyre where there is upwelling and the strengthened gyre over the sill where downwelling occurs.

linear stratification can produce large (~5 cm/s) flows simply as a result of incorrect specification of pressure terms. By carefully interpolating the equation of state to the grid point within the partial cell, it is possible to reduce these error flows by two orders of magnitude.

An additional improvement is realized by adding a bottom boundary layer to this formulation. The bottom boundary layer fills the bottom level of the model but is treated as though it lies immediately underneath the bottom-most ocean cell within the regular grid. The presence of such a thin layer allows for frictional dynamics to operate near the bottom, for the pressure gradient along the slope to be properly computed, and for dense flows to preserve their form as they move down a slope. At present, the partial cell bottom and bottom boundary layer have been implemented separately, though it is anticipated that they will be merged in the near future.

The effects of these changes are currently being tested in a number of model domains. The principal effect of including partial cells is to change the propagation of topographic waves. This can have major effects on the seasonal response of basins in which there is a gentle slope. One such basin is the Bay of Bengal. A 1° model of the Indian Ocean north of 30°S was constructed with 15 levels in the vertical. The bottom-most level is 700 metres thick. The model was initialized with Levitus temperature and salinity and forced with seasonally varying Hellerman winds and surface resorting back to Levitus. After 3 years, the annual pattern repeats clearly. The zonally averaged streamfunction in the eastern and western parts of the basin from the fifth year of the simulation is shown in Fig. 1. The upper row shows the streamfunction averaged over the western part of the basin (from 38° to 75°E), which includes the Somali Current region. A strong transport reversal is seen in both cases, but there are differences. In particular the centre of the Somali Current gyre shifts from 7°N in the full cell case to 4°N in the partial cell case, and the intensity of the gyre also increases. The bottom row shows the annual cycle of zonally averaged streamfunction in the northeastern Indian Ocean. Noticeable differences can be seen north of 10°N (in the Bay of Bengal) where the partial cell case produces a gyre-averaged minimum of 4 Sv in April, 25% larger than the full cell case.

The bottom boundary layer has principally been used thus far in idealized basins. Fig. 2 shows results from one such run, a domain spanning 60 degrees of longitude and running from the equator to 60°N. A 500 m deep sill at 45°N divides this domain into two basins, a shallow northern

basin approximately 200 m in depth and a deep southern basin 4000 m deep. The entire domain is initialized at 12°C and is run out for 160 years with the surface restored to the zonally averaged surface temperatures from the Levitus dataset. No wind stress is applied to the domain, so that the resulting circulation represents the density-forced flow only. Additionally, explicit horizontal mixing is turned off so that the only source of mixing is truncation errors in the advection equation, convection, and vertical diffusion. In the absence of a bottom boundary layer, cold water piles up behind the sill and the deep waters are all between 11° and 12°C. With a bottom boundary layer, there is strong flow down the slope, the thermocline is compressed, and the deep water is noticeably colder. As the additional flow down the slope upwells in the southern basin, the result is to increase the strength of the density-driven component of the subtropical gyre by a factor of 2. The bottom boundary layer clearly plays an important role in determining the overall density structure of this test basin.

Taken together, the bottom boundary layer and partial cell bottom offer the hope of accurately representing flows around both gentle and steep slopes while retaining relatively coarse vertical resolution in the ocean interior. As the model runs presented here indicate, such flows can play an important role in determining the response of the ocean to surface forcing as well as the mean structure. It is our hope that the new code will prove useful in exploring a wide range of problems of general interest in the oceanographic community.

References

Adcroft, A., C. Hill, and J. Marshall, 1997: Representation of topography by shaved cells in a height coordinate ocean model. Monthly Weather Review in press.

Bryan, K., 1969: A numerical method for the study of the circulation of the world ocean. Journal of Computational Physics, 4, 347–376.

Cox, M. D., 1984: A primitive equation, 3-dimensional model of the ocean. GFDL Ocean Group Technical Report No. 1.

Gerdes, R., 1993: A primitive equation ocean general circulation model using a general vertical coordinate transformation: 1 Description and testing of the model. J. Geophys. Res., 98, 14683–14701.

Pacanowski, R. C., 1996: MOM 2 Documentation, User's Guide and Reference Manual". GFDL Ocean Technical Report #3.1, Geophysical Fluid Dynamics Laboratory/NOAA, Princeton, USA.

Pacanowski, R. C., K. Dixon, and A. Rosati, 1991: The GFDL modular ocean model user guide. The GFDL Ocean Group Technical Report No.2, Geophysical Fluid Dynamics Laboratory, Princeton, USA, 16 pp.

Semtner, A. J., 1974: An oceanic general circulation model with bottom topography. In Numerical Simulation of Weather and Climate, Technical Report No. 9, UCLA Department of Meteorology.

NSCAT Data Now Available Via FTP

The first batch of NSCAT data (L1.7, L2, L3) is now available via anonymous FTP from podaac.jpl.nasa.gov. It is in the pub/ocean_wind/nscat/ subdirectory. This data has been reprocessed based on the findings of the calibration/ validation team. Selected Wind Vector data (25 km) will be made available in the next 24 hrs. Batch 25, which covers the time period 19–26 February 1997, is now available. Batches, which consist of one week of data, will be added for both the period prior to this and for more recent dates. The users manual and read S/W are also available via FTP.

Over the coming weeks the data will be made available on a variety of media. In addition, an NSCAT on-line subsetting routine is soon to be available through the web.

Data Types

There are currently 5 types of data and, with the exception of the global backscatter data, all of the data is available via FTP. (Level 1.7 is only staged for short periods because of its size.) The data types are produced at different stages in the processing and all but one are "swath data" based on the satellite ground track and are organized in files of one revolution or "rev" each. The one exception is L3 data; a global, daily gridded wind map. All data is geolocated and timetagged. The data is not real-time; the most recent data is about two weeks old. Realtime data will be available through NOAA.

Types of data:

- Level 3 - ocean gridded wind map, 0.5 deg. res.
- Level 2 - ocean swath wind vectors, 50 km res.
- Level 1.7 - ocean-only backscatter, 25 km res.
- 25 km "Dunbar" - global backscatter, ocean swath wind vectors, 25 km res.
- SWV's - ocean swath Selected Wind Vectors, 25 km res.

Data Products

The data types have been grouped into products for effective distribution via tape and CD-ROM. To obtain a sample of NSCAT data on media other than FTP, place an order through the homepage order form

(http://podaac.jpl.nasa.gov/mail-orders.html).

(A reminder that much of the data will be available via FTP from podaac.jpl.nasa.gov and does not need to be ordered.)

The three data products are:

085 NSCAT scatterometer ocean wind products CD-ROM (JPL) (Contains Level 2, 3 and SWV's)

084 NSCAT scatterometer global 25 km sigma-0 and ocean winds (Dunbar)

066 NSCAT scatterometer science product, levels 1.7, 2, 3 (JPL) (Contains Levels 1.7, 2 and 3)

For more information or to order data, please see

http://podaac.jpl.nasa.gov

or contact podaac@podaac.jpl.nasa.gov. Data are free of charge.

Moored Measurement of the Indonesian Throughflow at the Southwestern Edge of the Philippine Sea

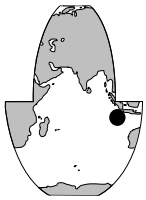

Hidetoshi Watanabe, Sanyo Techno Marine Inc., Tokyo 103, Japan; Yuji Kashino, JAMSTEC, Yokosuka 237, Japan; Hatsuyo Yamaguchi, Sanyo; Michio Aoyama, MRI, Tsukuba 305, Japan; Bambang Herunadi, Badan Pengkajian Dan Penerapan Teknologi, Jakarta 10340, Indonesia; Kentaro Ando, Kei Muneyama, and Humio Mitsudera, JAMSTEC; and Syaefudin, Badan Pengkajian Dan Penerapan Teknologi, Indonesia. lef04375@niftyserve.or.jp

Introduction

The net volume flux for the Indonesian Throughflow has been estimated for many years by observational studies and numerical simulations. Recent observational studies gave a wide range of estimates (from 7 to 18.6×10^6 m^3 s^{-1}) for the Indonesian Throughflow (Gordon and Fine, 1996). Furthermore, some numerical studies on the seasonal variability of ocean circulation around the Indonesian Islands indicated large seasonal transport variations (Masumoto and Yamagata, 1993, Miyama et al., 1995). It is found that various currents (i.e., the North Equatorial Current, the Mindanao Current, the South Equatorial Current, and the North Equatorial Counter Current) interactively flow and form the Mindanao Eddy and Halmahera Eddy in the southern part of the Philippine Sea, the entrance of the Indonesian Throughflow (Lukas et al., 1991). However, sufficient observational studies on the variability of the currents in this region have not been performed.

In this report, we show the preliminary results of the moored observation of the current, temperature and salinity between Talaud and Morotai islands from February 1994 through April 1995.

Observations

The two moorings were deployed between Talaud and Morotai Islands (Table 1 and Fig. 1) on 21 and 22 February 1994 during the RV Kaiyo PR24/PR1S cruise and were

Table 1. Locations of moored observation

Deployment Date	Stn.	Lat./long.	Depth
21 Feb. 1994	TMN	04 01.2°N, 127 30.6°E	2570m
22 Feb. 1994	TMS	03 10.8°N, 128 27.4°E	2277m

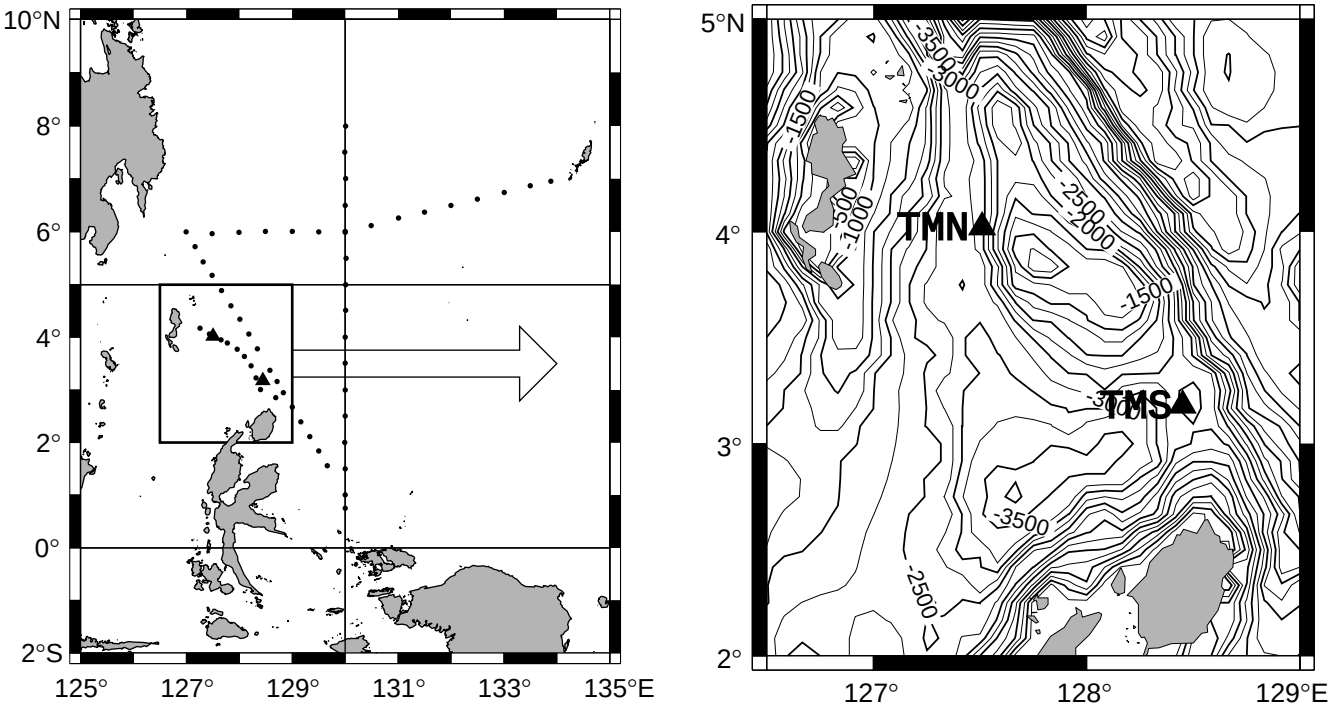

Figure 1. Location of mooring stations (left panel) and bottom topography surrounding the mooring stations (right panel). Solid triangle: mooring stations TMN and TMS. Solid circle: CTD/Rosette stations for PR24/PR1S/6N in 1994 Kaiyo WOCE cruise.

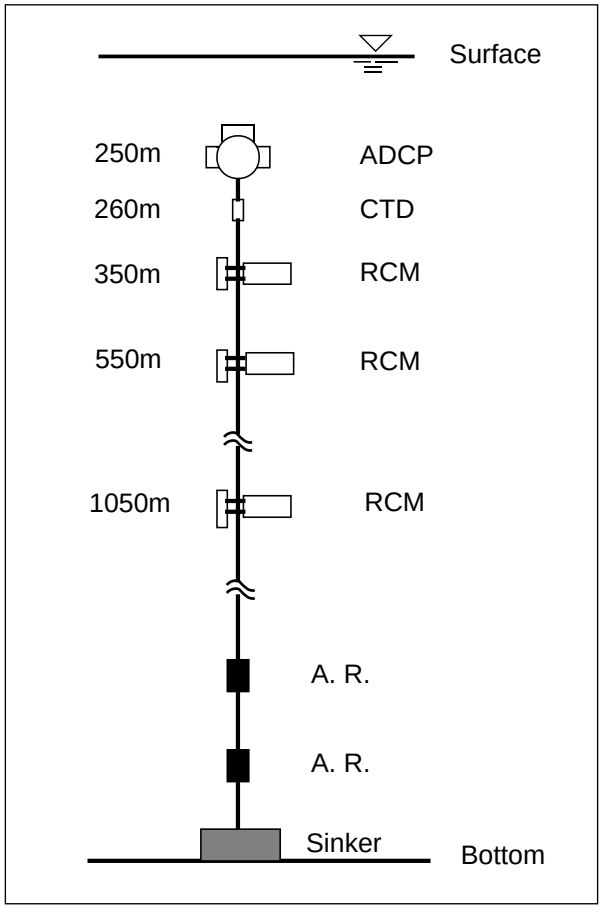

Figure 2. Mooring line.

recovered on 3 July 1995 (Report for the moorings deployed during Kaiyo-WOCE cruises between Talaud and Morotai Islands, 1996; Kawano et al., 1995; Kashino et al., 1996).

As shown in Fig. 2, each mooring was designed to have one upward-looking self-contained broad-band Acoustic Doppler Current Profiler (SC-BBADCP) at 250 m depth; one CTD (SBE16) at 260 m depth; and three Aanderaa current meters (RCM) at 350 m, 550 m and 1050 m depth. Temperature sensors were installed in all RCMs, conductivity sensors were installed in three RCMs (TMN-350 m, TMS-350 m, and TMS-550 m), and pressure sensors were installed in two RCMs (TMN-1050 m and TMS-1050 m).

We could not obtain the ADCP data because of an ADCP system program bug. The RCM data were acquired and filled the memory on 30 April 1995. Consequently, we could obtain hourly data on current velocity, temperature and salinity by RCMs from 21 or 22 February 1994 through 30 April 1995, and of temperature and salinity data from CTDs from 21 or 22 February 1994 through 3 July 1995 every 30 minutes.

Variabilities of the current, temperature and salinity

Diurnal or semi-diurnal tidal current was observed in the raw data. The amplitudes were estimated to be 5.9 cm/s for K1, 3.7 cm/s for 01, 2.7 cm/s for M2 and 0.3 cm/s for S2 tidal constituents of the 350 m depth at Stn.TMN.

In order to clarify the variability of current, temperature and salinity on a longer time scale than diurnal, we filtered out the fluctuations shorter than diurnal tidal current using a 48-hour Tide Killer Filter (48tk) designed by Hanawa and Mitsudera (1985).

The low-pass filtered time series of current velocity, temperature and salinity acquired by RCMs and CTD, and pressure acquired by CTD are shown in Fig. 3 for Stn.TMN and Fig. 4 for Stn.TMS. The low-pass residual currents appear to vary with time scales exceeding two to three months and about two months, but the direction and velocity of each time scale at the stations were different. At Stn.TMN, strong current at 350 m depth flows mainly northward with a velocity of about 30 cm/s. However, weaker current periods were observed from March 1994 through July 1994. At the deeper layers, the current velocity is not as great as at 350 m depth, and the current frequently flows to the southward, in the opposite direction to that at 350 m depth. At a depth of 350 m at Stn.TMS, a northwestward current was dominant from November 1994 through March 1995, and the same current was observed at a depth of 550 m. From February 1994 through October 1994, the currents at 350 m and 550 m depths tend to flow mainly westward, and that at 1050 m tends to flow mainly eastward, but the velocities are not so fast as observed after November 1994.

It should be noted that the "knockdown" of the moorings observed at Stn.TMS from November 1994 through April 1995 varied remarkably from 260 dbar to

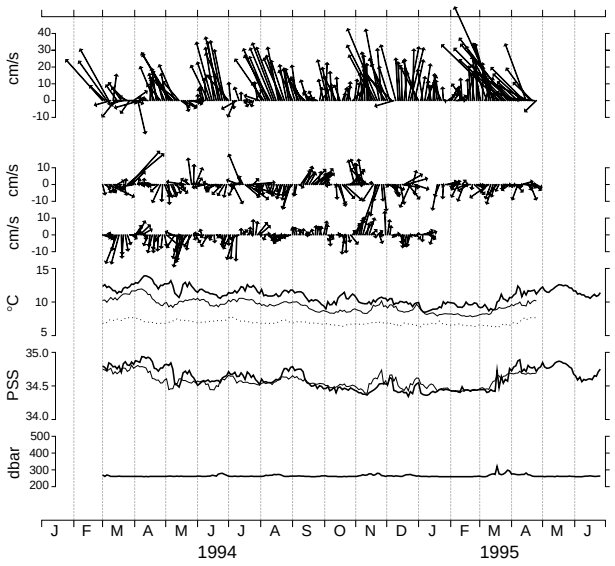

Figure 3. (top three) Velocity, low-pass filtered, drawn as sticks, (bottom three) water temperature, salinity and pressure on mooring TMN. Velocities are shown at depths 350, 550 and 1050 metres, from the top down, while thick line, thin line and dotted line are at the depths 260, 350 and 550 metres in temperature, salinity and pressure panel. A stick pointing upward indicates a velocity in north direction.

about 500 dbar. This is the period when the strong northwestward current was dominant at depths of 350 m and 550 m. Furthermore, around this period, low salinity water was observed and frequently showed less than 34.5 psu. This low salinity water probably originated from the North Pacific because of its low salinity. Considering the vertical section along 130°E observed in February 1994 and the currents shown in Fig. 4, this low salinity water might originate in the North Pacific and be transported by the strong northwest current associated with the Halmahera Eddy located northeast of Halmahera Island.

Seasonal current variation

To understand the constitution of the current fluctuation, power spectra for the northward and eastward low-pass filtered current velocities were calculated (Fig. 5). Significant spectral peaks are found at periods of around two months at 350 m and 550 m depth at Stn.TMN, and around one month at 1050 m. However, dominant spectral peaks are not found at Stn.TMS. In order to estimate the seasonal variation of the current, fluctuations with a period shorter than 120 days were filtered out. Stick diagrams of this low-pass filtered time series of current velocity are shown in Fig. 6. As mentioned previously, the Stn.TMN current at 350 m depth continuously flowed northwest-northward with a velocity of about 20 to 30 cm/s, except from April to May 1994. When the northward current was dominant at a depth of 350 m, it appeared to flow southward at a depth of 550 m, but the velocity was less than 10 cm/s. Current at a depth of 1050 m flowed mainly southward at a few cm/s from March to July 1994. After that, very weak flow was observed.

At the 350 m depth of Stn.TMS, low-pass current velocity varied, flowing northwestward from March to July 1994, turning southward from August to September 1994, and returning northwestward at 20 to 40 cm/s from

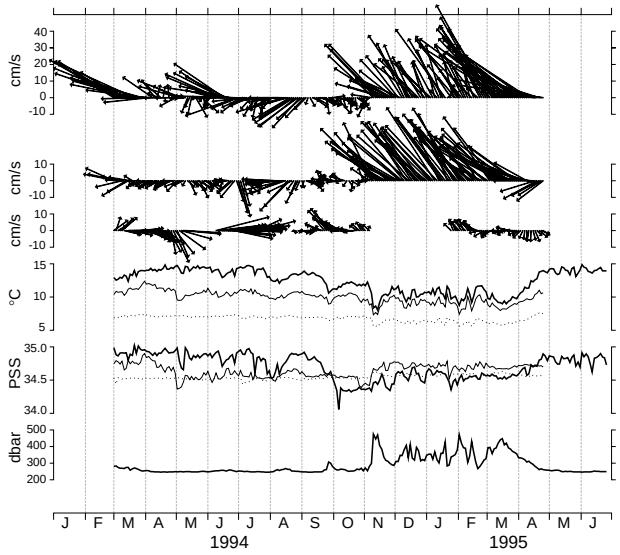

Figure 4. Same as Figure 3, but at the station TMS.

November 1994 through March 1995. The current characteristics after November 1994, when the inclination of mooring was observed, were clearly different from before, flowing continuously at a velocity of 30 cm/s or more, and sometimes over 40 cm/s in March 1995. At a depth of 550 m, current velocity varied, flowing westward in March 1994, from southeastward to southward from April to June 1994, and northwestward at a higher velocity similar to that at 350 m depth after November 1994. Current velocity at 550 m depth exceeded that at 350 m depth from December 1994 to January 1995, and it decreased slower than that at 350 m depth after February 1995. We consider that these strong northwestward currents might be a part of a clockwise Halmahera Eddy, but not the New Guinea Coastal Undercurrent, because of its water property. However, the current at 1050 m depth tended to flow in the

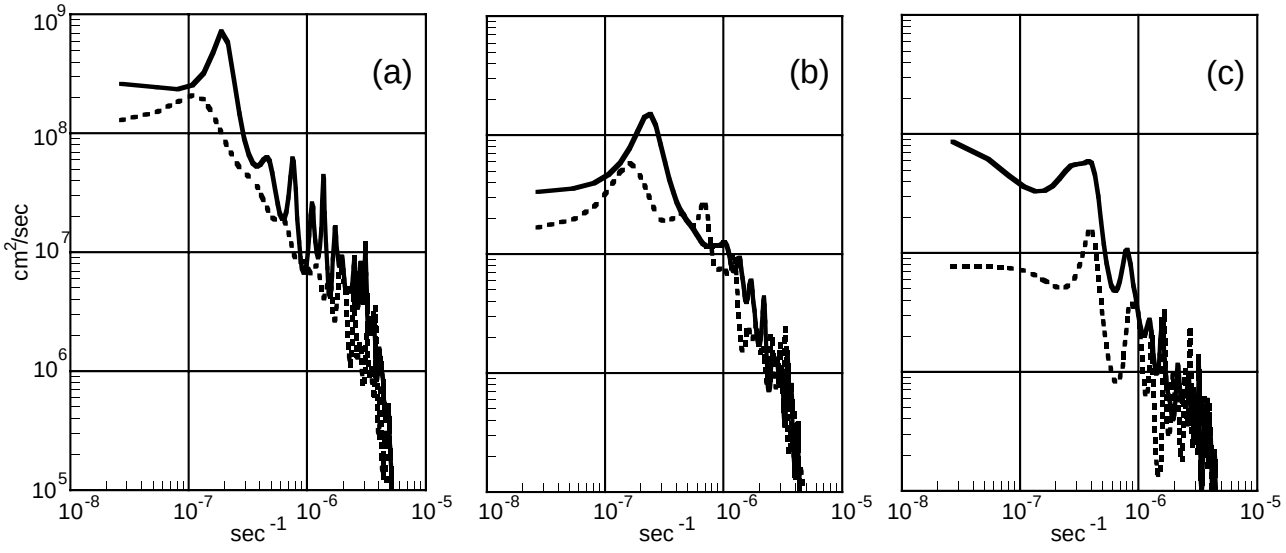

Figure 5. Power spectra for the northward (solid line) and eastward (dashed line) current velocity low-pass filtered by 48tk on mooring TMN at depths 350 m (a), 550 m (b) and 1050 m.

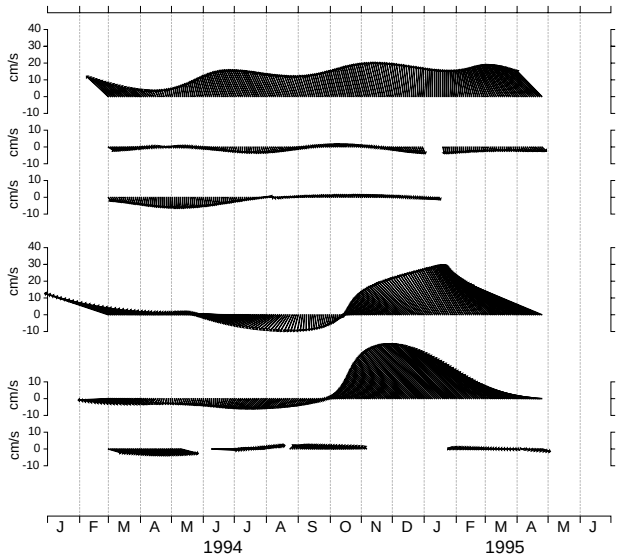

Figure 6. Velocity, low-pass (less than 120 days) filtered, drawn as sticks on moorings TMN (top three) and TMS (bottom three) at depths 350, 550 and 1050 metres from the top down for each mooring. A stick pointing upward indicates a velocity in north direction.

opposite direction to that at 350 m depth, flowing southeastward from March to July 1994, northwestward from September to October 1994.

Fluctuations with a time scale of around two months

The fluctuations at a time scale of around two months were examined on the band-pass time series between 30 days and 120 days. Fig. 7 shows the stick diagrams of these band-pass filtered time series of current velocities. They appear to fluctuate with a period of about two months, and the amplitude of velocity at both stations was about 20 cm/s at 350 m depth and about 10 cm/s at the other layers. One of the remarkable features is that the phase of fluctuations with a period of about two months have opposite phases between 350 m depth and the other layers at Stn.TMN, while the current fluctuates with similar phases in the three layers at Stn.TMS. The wind stress due to monsoon, the barotropic or baroclinic mode due to the Rossby wave, and proper oscillation due to the topography around this region may cause this scale of fluctuation. The relationship between current and wind variations will be studied by one of the authors in the near future.

Summary

Preliminary results of the moored observation conducted between Talaud and Morotai Islands are summarized below.

(1) The current in this region varied with a time scale exceeding two or three months (seasonal change), about two months, and shorter than diurnal variations (tidal currents).

(2) The seasonal variability at Stn.TMN is such that the current flowed mainly northward at a depth of 350 m and southward at depths of 550 m and 1050 m. At Stn.TMS, the current at depths of 350 m and 550 m flowed northwestward or southward, and continuously flowed northwestward at a velocity exceeding 30 cm/s from November 1994 through March 1995. However, the current at 1050 m tended to flow in the opposite direction to that at 350 m from March through October 1994.

(3) Fluctuations with a period of about two months were evident at both stations. The amplitudes of velocity were about 20 cm/s at 350 m depth and 10 cm/s at other layers. The phase appeared to be reversed between 350 m depth and the other layers at Stn.TMN, while it had similar phases in the three layers at Stn.TMS.

(4) When a northwestward current was dominant at 350 m and 550 m of Stn.TMS from November 1994 through March 1995, low-salinity water (less than 34.5 PSS) was observed. This low-salinity water might originated in the North Pacific and be transported by the Halmahera Eddy.

Acknowledgements

The authors thank all participants of the cruises and Captain Tanaka and his crew of the RV Kaiyo. This study was executed based on a collaborative ocean research framework between the Japan Marine Science and Technology Center (JAMSTEC) and Badan Pengkajian Dan Penerapan Teknologi, Indonesia (BPPT) exsisting since 1992. A part of this study was performed using Special Coordination Funds of the Science and Technology Agency of the Japanese Government.

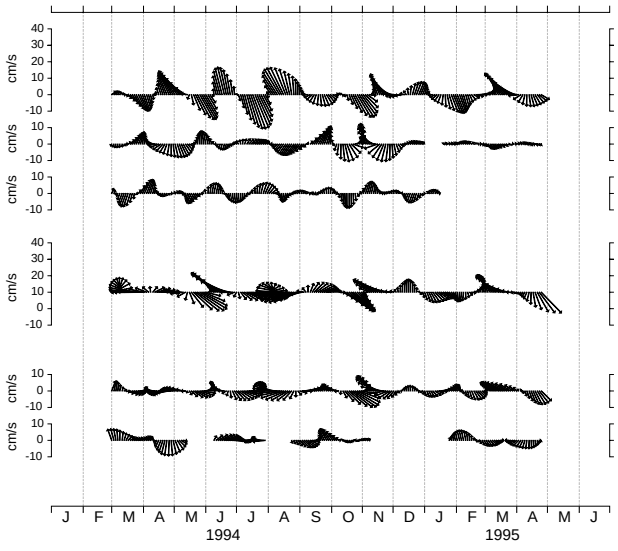

Figure 7. Same as Figure 6, but band pass (30 days through 120 days) filtered time series.

References

Gordon, A. L., and R. A. Fine, 1996: Pathway of water between the Pacific and Indian oceans in the Indonesian seas. Nature, 379, 146–149.

Hanawa, K., and H. Mitsudera, 1985: On the Data Processings of Daily Mean Values of Oceanographical Data. Note on the Daily Mean Sea-Level Data. Bulletin on Coastal Oceanography, Vol. 23, No. 1, 79–87. (in Japanese)

Kawano, T., N. Hendiarti, Y. Anantaesana, Y. Kashino, Syaefudin, K. Muneyama, M. Aoyama, and K. Ando, 1995: A Hydrography in the Southern Philippine Sea: From WOCE Hydrographic Programme Section PR1S and PR24. International WOCE Newsletter No. 19, 11–14.

Kashino, Y., M. Aoyama, T. Kawano, N. Hendiarti, Syaefudin, Y. Anantasena, K. Muneyama, and H. Watanabe, 1996: The water masses between Mindanao and New Guinea. J. Geophys. Res., 101, 12391–12400.

Lukas, R., E. Firing, P. Hacker, P. Richardson, C. Collins, R. Fine, and R. Gammon, 1991: 'Observations of the Mindanao Current' during the Western Equatorial Pacific Ocean Circulation Study. J. Geophys. Res., 96, 7089–7104.

Masumoto, Y., and T. Yamagata, 1993: Simulated Seasonal Circulation in the Indonesian Seas. J. Geophys. Res., 98, 12501–12509.

Miyama, T., T. Awaji, K. Akitomo and N. Imasato, 1995: Study of seasonal transport variations in the Indonesian seas. J. Geophys. Res., 100, 20517–20541.

On the Maintenance and Initiation of the Intraseasonal Oscillation: A Coupled Ocean-Atmosphere Phenomenon?

Kenneth R. Sperber, PCMDI, Lawrence Livermore National Laboratory, Livermore, CA 94551; and Julia M. Slingo, Centre for Global Atmospheric Modelling, University of Reading, Reading, RG6 6BB, UK. ken@met.reading.ac.uk

The Madden-Julian Oscillation (hereafter referred to as the intraseasonal oscillation) is a dominant mode of variability in the tropics (Madden and Julian 1971, 1972). It is manifested on a time scale of ~30-60 days through large-scale circulation anomalies, which occur in conjunction with eastward evolving convective anomalies. These features are strongest and most coherent during boreal winter/spring when the west Pacific warm pool is centered near the equator. Characteristics of the life cycle of intraseasonal oscillations (IO) have been described by many authors (e.g., Knutson and Weickmann, 1987; Rui and Wang, 1990; Matthews, 1993; Hendon and Salby, 1994).

Satellite derived outgoing longwave radiation (OLR) and reanalysis from the National Centers for Environmental Prediction/National Center for Atmospheric Research (NCEP/NCAR, Kalnay et al., 1996) are used to test the theories of evaporative wind feedback (Emanuel, 1987; Neelin et al., 1987) and frictional wave-CISK (Conditional Instability of the Second-Kind, Hendon and Salby, 1994) for the maintenance and initiation of the IO. We consider November 1987 through May 1988, a period of strong IO activity. Sperber et al. (1997) present an extended version of this paper, and examination of the IO in 15 atmospheric general circulation models is given in Slingo et al. (1996).

In Fig. 1 (page 20), lagged correlation analysis has been used to demonstrate the eastward propagation of key variables associated with the IO. The lagged correlations are calculated with respect to an IO index of pentad averaged 20–100 day bandpass filtered 200 hPa velocity potential from the NCEP/NCAR reanalysis. The IO index has been averaged over the region 100°-140°E, 10°N–10°S. Sperber et al. (1997) demonstrate that this index is an excellent measure of IO variability. In the left-hand panel, correlations of this IO index with total OLR are plotted as isolines. At day -15, enhanced convection (blue isolines) is apparent over the western tropical Indian Ocean. During days -10 and -5 the enhanced convection intensifies, encompassing much of the central/eastern Indian Ocean. By day 0 and day +5 the enhanced convection is found over the western Pacific Ocean, and it extends southward over Australia. At subsequent time lags the enhanced convection weakens as it makes its way into central Pacific and southward into the South Pacific convergence zone. Prior to, and subsequent to convection over the Maritime continent suppressed convection is noticed (red isolines).

A main tenet of the evaporative wind feedback mechanism is that evaporation to the east of the convection is the dominant source of moisture. To investigate the viability of this theory we have correlated the IO index with bandpass filtered latent heat flux from the NCEP/NCAR reanalysis. From day -5 onward, when the convective signature is readily apparent, the correlations indicate that evaporation is enhanced to the west of the convection, and it is below normal to the east of the convection. These results are consistent with observations from the Tropical Ocean Atmosphere (TAO) array in the western Pacific (Zhang, 1996; Lau and Sui, 1997), and indicate that evaporative wind feedback is not the dominant process by which the eastward propagation of the IO is maintained. In frictional wave CISK, convergence (negative divergence) at the surface is displaced approximately 40° to the east of that at 850 hPa. We have examined bandpass filtered divergence and streamfunction from the reanalysis, and find that the contribution by frictional convergence is not apparent.

Recent results have suggested that air-sea interactions may be important for maintaining the eastward propagation of the IO (e.g. Gutzler et al., 1994; Chen et al., 1996; Zhang,

1996; Lau and Sui, 1997). To examine this hypothesis in more detail, in the first sequence of panels in Fig. 1 we also show correlations of the IO index with bandpass filtered SST. On day -15 convection over the tropical western Indian Ocean occurs over above normal SST. Warmer SSTs are also found near the equatorial central Indian Ocean and Sumatra, which at day -10 is where the convection is the strongest. On day -10 warm SST anomalies develop south of the Indonesian peninsula, near 115°E, 15°S, which is precisely where suppressed convective activity (and presumably enhanced subsid-ence) occurred during the previous pentad (day -15). On day -5 the convection extends eastward over New Guinea and adjacent to northwest Australia, where above normal SST and suppressed convection were found on day -10. This cycle continues on day 0, where convection north of New Guinea is manifested. On day +5 through day +15 convection is found near 170°E, 5–20°S where warm SST anomalies developed previously, subsequent to suppressed convection.

In the vicinity of the convection, enhanced latent heat flux (and perhaps cloud shielding) serve to cool the local SST, resulting in a zonal gradient of SST with warmer values to the east which may provide the impetus for convection to develop further east. West of the convection, where below normal SST coincides with the enhanced latent heat flux, particularly over the Indian Ocean from day 0 through day +10, the western limit of the convection is eroded. These results suggest that it is the local gradient of SST that is important for the eastward migration of the IO. This cycle of suppressed convection east of the convection, leading to increased SSTs and eastward migration of the convective envelope at subsequent pentads, with conditions in the west that serve to decrease SSTs and convection, is consistent with the conceptual model of Flatau and Flatau (1996) for maintaining eastward propagation of the IO, and with observations from the western Pacific Ocean (Zhang, 1996; Lau and Sui, 1997).

A major caveat of this work is that few, if any, Indian Ocean observations were incorporated into the reanalysis (personal communication, Burridge, 1996). Therefore the latent heat flux from the reanalysis is not constrained by observations, and it is a product of the model parametrization. Extending the TOGA-TAO array into the Indian Ocean would be beneficial for understanding ocean-atmosphere interactions over this region, and for studying transitions between the Indian Ocean and the western Pacific.

Acknowledgements

Special thanks to the NCEP/NCAR for making the reanalysis data set available, and the ECMWF for making the observed SST and reanalyzed skin temperature data available. We thank Drs Jim Boyle (PCMDI/LLNL) and William K.-M. Lau for useful discussions, Dr Harry Hendon (University of Colorado) for providing the observed OLR data, Dr Mike Fiorino (PCMDI/LLNL) for facilitating access to the NCEP/NCAR reanalysis, and Dr Mike Pedder (University of Reading) for supplying the code for the computation of the filter weights. This work was performed under the auspices of the US Department of Energy Environmental Sciences Division at the Lawrence Livermore National Laboratory under contract W-7405-ENG-48.

References

Chen, S. S., R. A. Houze, and B. E. Mapes, 1996: Multiscale variability of deep convection in relation to large-scale circulation in TOGA COARE. J. Atmos. Sci. 53: 1380–1409.

Emanuel, K. A., 1987: An air-sea interaction model of intra-seasonal oscillations in the tropics. J. Atmos. Sci. 44: 2324–2340.

Flatau, M. and P. J. Flatau, 1996: The role of SST feedback in the development of equatorial convection. Proceedings of the AMS Conference on the Global Ocean-Atmosphere-Land System (GOALS), Atlanta, Georgia, J124–J127.

Gutzler, D. S., G. N. Kiladis, G. A. Meehl, K. M. Weickmann, and M. Wheeler, 1994: The global climate of December 1992-February 1993. Part II: large-scale variability across the tropical western Pacific during TOGA COARE. J. Clim. 7: 1606–1622.

Hendon, H. H. and M. L. Salby, 1994: The life cycle of the Madden-Julian oscillation. J. Atmos. Sci. 51: 2225–2237

Kalnay, E., M. Kanamitsu, R. Kistler, W. Collins, D. Deaven, L. Gandin, M. Iredell, S. Saha, G. White, J. Woollen, Y. Zhu, M. Chelliah, W. Ebisuzaki, W. Higgins, J. Janowiak, K. C. Mo, C. Ropelewski, J. Wang, A. Leetmaa, R. Reynolds, R. Jenne, and D. Joseph, 1996: The NCEP/ NCAR 40-year reanalysis project. Bull. Amer. Meteorol. Soc. 77: 437–471.

Knutson, T. R. and K. M. Weickmann, 1987: 30–60 day atmospheric oscillations: composite life cycles of convection and circulation anomalies. Mon. Wea. Rev. 115: 1407–1436.

Lau, K.-M. and C. H. Sui, 1997: Mechanisms of short-term sea surface temperature regulation: observations during TOGA-COARE. J. Clim. 10: 465–472.

Madden, R. A. and P. R. Julian, 1971: Detection of a 40–50 day oscillation in the zonal wind in the tropical Pacific. J. Atmos. Sci. 28: 702–708.

Madden, R. A. and P. R. Julian, 1972: Description of global-scale circulation cells in the tropics with a 40–50 day period. J. Atmos. Sci. 29: 1109–1123.

Matthews, A. J., 1993: The intraseasonal oscillation. Ph.D. Dissertation, Department of Meteorology, University of Reading, Reading, UK.

Neelin, J. D., I. M. Held, and K. H. Cook, 1987: Evaporation-wind feedback and low-frequency variability in the tropical atmosphere. J. Atmos. Sci. 44: 2341–2348.

Rui, H. and B. Wang, 1990: Development characteristics and dynamic structure of tropical intraseasonal convective anomalies. J. Atmos. Sci. 47: 357–379.

Slingo, J. M., K. R. Sperber, J. S. Boyle, J.-P. Ceron, M. Dix, B. Dugas, W. Ebisuzaki, J. Fyfe, D. Gregory, J.-F. Gueremy, J. Hack, A. Harzallah, P. Inness, A. Kitoh, W. K.-M. Lau, B. McAvaney, R. Madden, A. Matthews, T. N. Palmer, C.-K. Park, D. Randall, and N. Renno, 1996: Intraseasonal oscillations in 15 atmospheric general circulation models: Results from an AMIP diagnostic subproject. Clim. Dyn. 12: 325–357.

Sperber, K. R., J. M. Slingo, P. M. Inness, and W. K.-M. Lau, 1997: On the maintenance and initiation of the intraseasonal oscillation in the NCEP/NCAR reanalysis and the GLA and UKMO AMIP simulations. Clim. Dyn. (in press).

Zhang, C., 1996: Atmospheric intraseasonal variability at the surface in the tropical western Pacific Ocean. J. Atmos. Sci. 53: 739–758.

North Atlantic Anticipates Biggest Float Fleet Ever

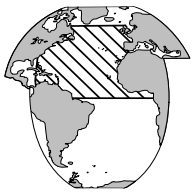

Walter Zenk, Institut für Meereskunde, Universität Kiel, Germany.
wzenk@ifm.uni-kiel.de

In February 1997 the Ocean Observing Panel for Climate (OOPC) met at the University of Cape Town under its chairman Neville Smith. This group of experts was esrablished in 1996 jointly by the Global Ocean Observing System (GOOS), the Global Climate Observing System (GCOS) and the World Climate Research Programme (WCRP). Its terms of reference are to monitor, describe and understand the physical and biogeochemical processes that determine the ocean circulation. Among other issues the Panel also reviewed future float experiments in the North Atlantic.

In preparation for the meeting I had collected information on all US and European float experiments in the North Atlantic started in 1996 or planned for 1997–1999. During the discussions in Cape Town it appeared that the list was incomplete. In the following weeks all potential experimentalists, who we thought would use floats, were asked to submit their plans by electronic mail. The community responded promptly which is highly appreciated. I had offered to circulate the results of my survey in return for the PI's helpful answers. Instead of individual answers I present the results here in Table 1 and Fig. 1.

The International WOCE Newsletter appears to be an excellent platform for the exchange of this comprehensive information on planned float experiments in the North Atlantic since the WOCE Float Planning Committee was disbanded before the major N. Atlantic experiments were started. This summary may serve as a reference for all float users inside and outside the WOCE community. (Those using RAFOS floats may contact Kevin Speer at IFREMER Brest (kevin.speer@ifremer.fr) for an up-to-date summary of moored sound generators in the eastern North Atlantic.)

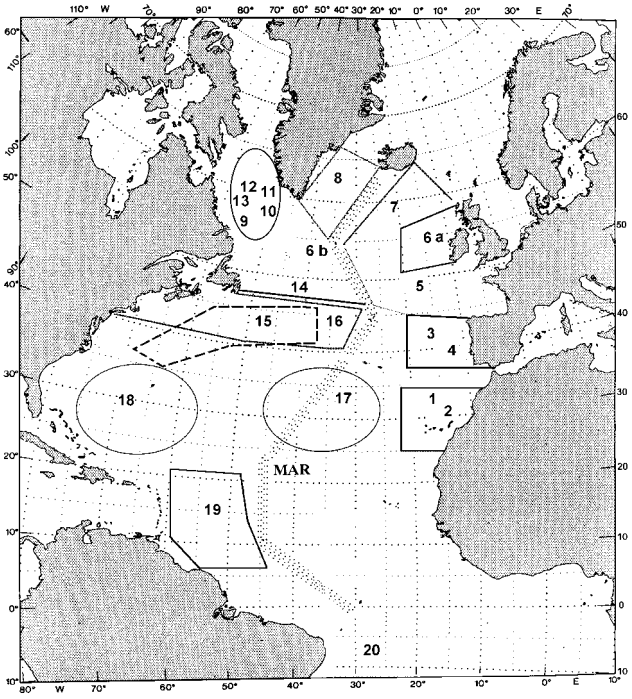

Figure 1. Regional distribution of experiments with various floats in the North Atlantic, 1996–99. Areas are numbered in accordance with column 1 in Table 1.

Table 1. Inventory of intended float deployments in the North Atlantic, 1996–99. Information was collected on the base of an electronic poll conducted in March 1997. It has been checked by B. Thompson from the WOCE Data Information Unit. The first column contains numbered areas which are reproduced in Fig. 1. The following abbreviations were used:

Instrumentation:

R	RAFOS (Ranging and Fixing of Sound) float, passive
M	French MARVOR float, active
A	ALACE (Autonomous Lagrangian Circulation Explorer), active
P-A	profiling ALACE with temperature sensor
S/P-A	profiling ALACE with temperature and conductivity sensors
AGP	German 'Automatischer Profilierender Geratetrager', (Automatic Profiling Platform), prototype

Other:

+	additional equipment is expected
?	information presently unavailable to the author
ACCE	Atlantic Circulation and Climate Experiment
ARCANE	a joint civil and military exercise in the eastern Atlantic by French institutions
ARI	Accelerated Research Initiative
CANIGO	European project 'Canary Island Azores Gibraltar Experiment'
MAR	Mid Atlantic Ridge
ONR	Office of Naval Research
PIRATA	Pilot Research Moored Array in the Tropical Atlantic
SAMBA	Subantarctic Motions in the Brazil Basin
SFB	German 'Sonderforschungsbereich' (Special Research Initiative)
SOC	Southampton Oceanography Centre

No.	PI/Project	Region/Coverage	Depth (m)	Float type	1996	1997	1998	1999	Sum
					Number of Intruments				
1	Knoll, Cantos/ CANIGO	Canary Basin	500	R		July/Aug 11			11
2	Zenk, Gould, Speer, Cantos/ EUROFLOAT	Canary Basin	1000	R	Oct'95 15	Jan 6			21
3	LeCann, Serpette, Speer/ARCANE ? French Navy ?	Iberian Basin	400	M	29	8?			37+
4	Ambar/CANIGO	Iberian Basin	800, 1000	R		June --> 14	10		24
5	Speer, Gould, Cantos/EUROFLOAT	Eastern Basin	1750	M	21				21
6 a,b	Richardson, Bower/ WOCE, ACCE	NE North Atlantic incl. east-boundary	σ_0= 27.5	R	Oct/Nov 14	June 34 Oct 20			68
7	Zenk, Siedler, Mueller/ SFB Kiel	Iceland Basin	~ 1400	R		May 20	summer 20+		40+
8	Gould/SOC	Irminger Sea	1500	(S)/P-A	7				7
9	Schott, Send,Rhein/ SFB Kiel	Labrador Sea	1500	(S)/P-A		Jan 6+			6+
10	Davis, Owens/ ONR Conv. ARI	Labrador Sea	350 - 1400	S/P-A with vanes	31	20	20		71
11	Rossby, Prater/ ONR Conv. ARI	Labrador Sea	?	R					?
12	D'Asaro/ ONR Conv. ARI	Labrador Sea	?	special purpose					?
13	Freeland/ ?	Labrador Sea	?	P-A	fall 5				5
14	Koltermann,Knutz/ WOCE, ACCE	W of MAR, 47°N	1500	S/P-A APG-new		June 3 ?	3?		6+
15	Rossby, Carr, Prater/ WOCE	Gyre Exchange N. Atlantic Current and on 38°W	σ_0=27.5	R from VOS		spring 80			80
16	Davis, Owens/ WOCE	N of 40°N 2x2 grid	600 (-1400)	(S)/P-A with vanes	fall 40	Feb/Mar 30	Jan/Feb 30		100
17	Leeman, Molinari/ ?	S of 40°N 600 km^2	800 -1000	A and P-A		summer 19 fall 17	18		54
18	Riser/ ?	Sargasso Sea	1000	P-A		summer 20	30	20	70
19	Schmitt/ ?	6°N-16°N 600 km^2	1000	S/P-A		summer 10	30		40
20	Ollitrault,Schopp, Servain, Vianna, McPhaden/ SAMBA, PIRATA	Equator 15°N to 10°S	partly ~ 800	M					?

Had we expected 661 and more floats to be on mission between 1996 and 1999 in one ocean basin? By oceanographic standards this certainly is not a small number! Float technology is now mature for observations of current within the oceans.

It is interesting to recall the float data requirements for WOCE in its Implementation Plan from 1988. The authors of this document considered floats primarily as a means of providing the best velocity reference for use with hydrography. They sought a global mapping strategy at mid-level below the main pycnocline. Depths between 1500 and 2500 m were recommended as having low eddy noise, with small interference from topography, and optimal acoustic transmission conditions.

It is very pleasing to see that the total number of planned floats in the North Atlantic approaches the requirements for most of the WOCE aspects. The Implementation Plans suggested 5 float years in every $500\,\mathrm{km} \times 500\,\mathrm{km}$ square in the ocean. If we assume the area covered in Fig. 1 of order $40 \cdot 10^6\ \mathrm{km}^2$ then this would require 160 floats surviving 5 years or 800 float years.

Acknowledgement

The Bundesministerium für Bildung, Wissenschaft, Forschung und Technologie (03F0157A) and the Deutsche Forschungsgemeinschaft (SFB 460) have contributed substantially to the German float programme in the Atlantic.

Climatic Long-Term Interactions for the Mass-Balance in Antarctica

(CLIMA Project Group) PNRA, andreab@hydro.isdgm.ve.cnr.it*

Many important phenomena take place in the Southern Ocean, in particular in the zones of Antarctic Convergence and Divergence, on the continental shelf and on the slope. These areas are characterized by thermohaline fronts associated with relevant energy exchange with the atmosphere.

In the framework of the Italian National Program for Antarctic Research (PNRA), the Climatic Long-term Interactions for the Mass-balance in Antarctica project has been working for four years, focusing in the definition of the main aspects of the local and large scale circulation of the Ross Sea and on convection and diffusion of dense waters. Variability induced by the wind field, ice water budget, topographic effects influence the vertical stability of the water masses as well as heat exchange an ice coverage.

The contribution of the CLIMA project to understanding global change is based on "in situ" measurements, acquisition of remotely sensed data, modelling. Research activities are focused on the following topics:

- Hydrology and dynamics of the Southern Ocean.
- Modelling.
- Air-sea interaction and meteo-climatic forcing.
- Fluxes of suspended matter.

The Antarctic Circumpolar Current (ACC) is one of the most important current systems in the world ocean. Its eastward movement is constrained by important topographic features (Drake Passage, Pacific Antarctic Ridge, etc.) and limited to the south by a coastal countercurrent whose flow, opposite to the ACC, shows major deviations from a straight pattern in correspondence of the Weddel and Ross margin basins.

The dynamical system plays an important role in the ocean mass and heat budget as well as the air-sea exchange. Our project can contribute on the study of dynamical aspects of the circulation in the Southern Ocean, as well as on the relationships among physical, geochemical and biological (primary productivity) aspects in the area between

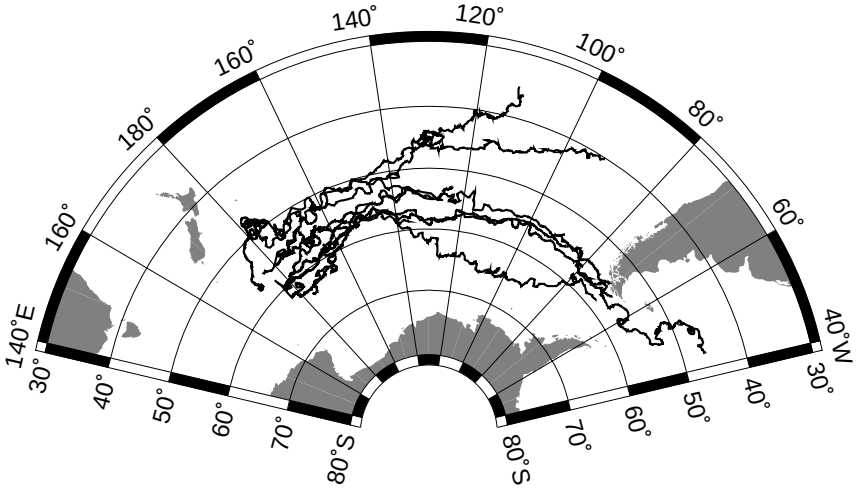

Figure 1. Trajectories of surface drifters deployed in the Southern Ocean in the framework of the PNRA activities. Data collected through October 1996.

*Programma Nazionale di Ricerche in Antartide. Coordinator: G. Spezie. Scientific Committee: A. Artegiani, A. Bergamasco, G. Manzella, S. Tucci.

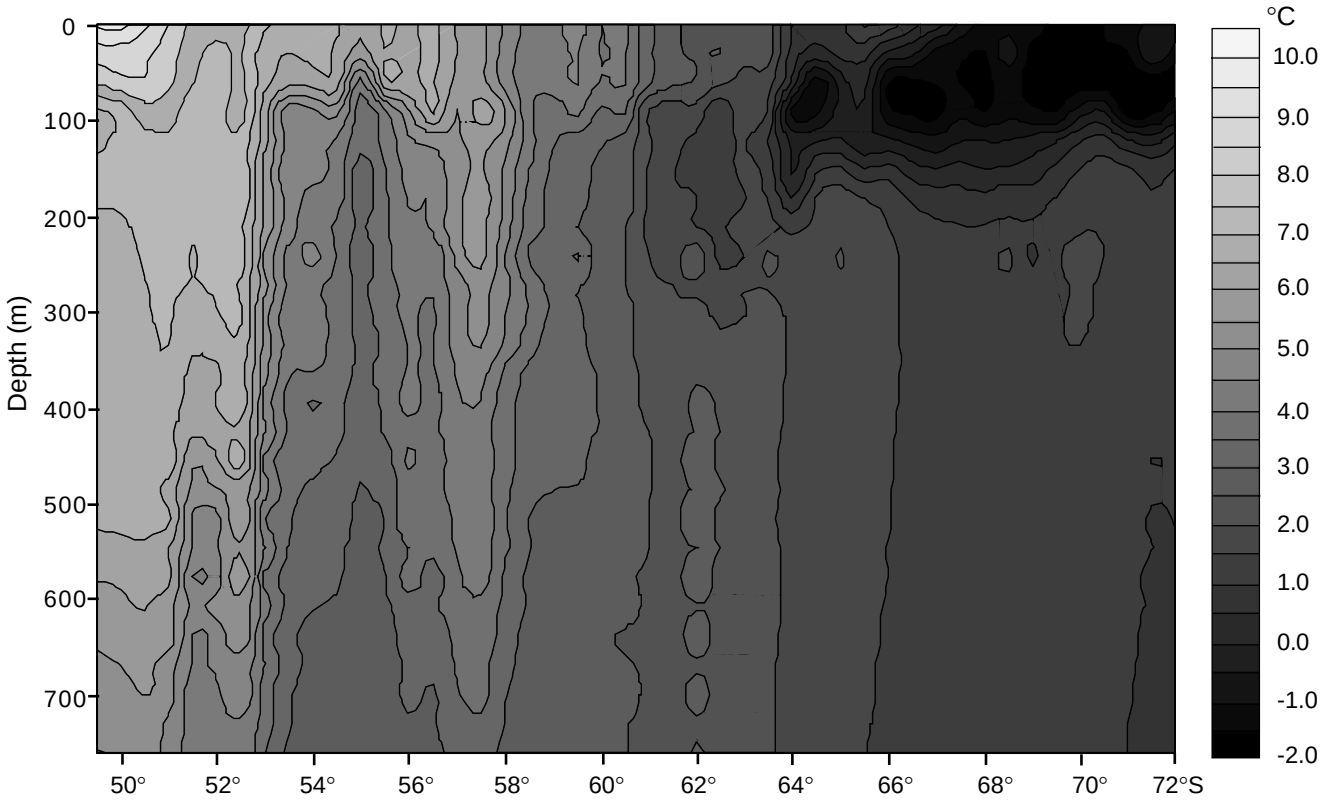

Figure 2. XBT section along 175°E (P14S WOCE transect) performed during last CLIMA expedition in Antarctica (1995–1996).

New Zealand and Ross Sea. A study of seasonal variability of the ocean dynamics is also part of the CLIMA project.

During the 93–94 expedition twelve surface and subsurface floats were deployed in the Southern Ocean along the route New Zealand–Cape Adare between 55–63°S and 170–175°E in order to better understand the detailed dynamics of the ACC. Surface drifters have proved to be a powerful tool for the description of the general circulation in the Southern Ocean. Furthermore, given our interest in the description and modelling of the circulation in the Ross Sea, drifter measurements provide us with the necessary boundary conditions both at the surface and at the offshore limit of the basin.

By means of Lagrangian instruments we have been investigating both the surface and subsurface dynamics of the studied area. In particular, as far as the surface is concerned, besides providing direct ones, these measurements well complements altimeter data giving us information concerning the non geostrophic component of the circulation in the upper layer.

On the other hand, the complexity of the internal dynamics has been explored by means of the set of subsurface floats. It is worthwhile to underline that we use ALACE floats i.e. pop-up floats which rise to surface every few days and transmit data and location through the ARGOS satellite service.

The usefulness of gathering additional data is due to extreme difficulties in carrying out hydrological measurements in the convergence zone, almost always characterized by very rough sea conditions, this suggests the necessity of mapping that specific area by means of readily deployable instruments or of Lagrangian ones.

Also in the framework of the CLIMA project two oceanographic surveys were carried out from January to February 1995 and 1996 with the Italian RV Italica. During these cruises from New Zealand to Ross Sea 10 drifting buoys were deployed which add to the 12 deployed earlier (Fig. 1). Besides, more than 600 XBT were launched in 6 times along the WOCE section P14 which links Cape Adare to New Zealand and along the continental slope of the Ross Sea (Fig. 2).

Three moorings were positioned, and are still working: one in the polynya of Terranova Bay and two in the ice shelf water core off the Ross Ice. Each mooring is fully equipped with ADCP, Aanderaa current meters, SBE T/C sensors, sediment traps and trasmissometers. More than 150 hydrological stations were carried out all over the Ross Sea to identify and follow the main diffusion paths of ISW (Ice Shelf Water) and HSSW (High Salinity Shelf Water). A SBE 9/11plus multiparameter sonde with SBE Carousel $24 \times 12l$ was used.

A new oceanographic campaign is scheduled in the austral summer 1997–1998, and the year after all the mooring will be definitely recovered and we will proceed to modelling the ocean circulation at different spatial and temporal scales.

Note on Copyright

WOCE is a component of the World Climate Research Programme (WCRP), which was established by WMO and ICSU, and is carried out in association with IOC and SCOR. The scientific planning and development of WOCE is under the guidance of the Scientific Steering Group for WOCE, assisted by the WOCE International Project Office.

The International WOCE Newsletter is edited by Roberta Boscolo (roberta.boscolo@soc.soton.ac.uk) at the WOCE IPO at Southampton Oceanography Centre, Empress Dock, Southampton, SO14 3ZH, UK, Tel: 44-1703-596789, Fax: 44-1703-596204, e-mail: woceipo@soc.soton.ac.uk,

http://www.soc.soton.ac.uk/OTHERS/woceipo/ipo.html

We hope that colleagues will see this Newsletter as a means of reporting work in progress related to the Goals of WOCE as described in the Scientific Plan.

The editor will be pleased to send copies of the Newsletter to institutes and research scientists with an interest in WOCE or related research.

Printed by the Design and Print Centre of the University of Southampton